culture plates and incubated with 2×10^5 human monocyte-derived macrophages (Effector:Target [E:T] = 1:10) in 1 mL of RPMI 1640 medium alone or with 10% heat-inactivated NHS for 24 h at 37°C. Following incubation, the target cells and human monocyte-derived macrophages were harvested with EDTA solution. The cells were counterstained with allophycocyanin-conjugated mouse monoclonal antibodies to human CD11c (BD Pharmingen) and washed and fixed with 2% formaldehyde-PBS. Two-color flow cytometric analysis was performed with a FACSCalibur flow cytometer under optimal gating. PKH67-labeled target cells were detected in the FL-1 channel and allophycocyanin-labeled human monocyte-derived macrophages were detected in the FL-4 channel. Dual-labeled cells ($PKH67^+/CD11c^+$) were considered to represent phagocytosis of targets by human monocyte-derived macrophages. Residual target cells were defined as cells that were $PKH67^+/CD11c^+$.

Adipogenic and osteogenic differentiation procedure

For adipogenic differentiation, cells were cultured in differentiation medium (Zen-Bio, Durham, NC). After 3 days, half of the medium was changed with adipocyte medium (Zen-Bio) every 2 days. Ten days after differentiation, characterization of adipocytes was confirmed by microscopic observation of intracellular lipid droplets by oil red O staining. Osteogenic differentiation was induced by culturing the cells in DMEM containing 10 nM dexamethasone, 50 mg/dL ascorbic acid 2-phosphate, 10 mM beta-glycerophosphate (Sigma, St. Louis, MO), and 10% FBS or heat-inactivated NHS. The differentiation was examined by alizarin red staining and alkaline phosphatase (AP) activity. For alizarin red staining, 7 or 18 days after differentiation, the cells were washed three times and fixed with dehydrated ethanol. After fixation, the cells were stained with 1% alizarin red S in 0.1% NH_4OH (pH 6.5) for 5 min and then washed with H_2O. AP activity was investigated at 2 weeks after differentiation using the procedure described previously.[26] AP activity per cell was calculated based on the amount of DNA. DNA content was measured by a modification of the method of Labarca and Paigen.[27]

Statistics

Values are given as the mean ± standard deviation. Student's t-test was used to ascertain the significance of differences within groups. Differences were considered statistically significant when $p < 0.05$. All statistical analyses were performed using the SPSS Statistics 17.0 package (SPSS, Chicago, IL).

Results

Presence of Neu5Gc and human natural preformed antibodies binding to hADSCs/MSCs

First, the specificity of chicken anti-Neu5Gc polyclonal antibody was examined (Fig. 1A). Flow cytometric analysis showed that chicken anti-Neu5Gc polyclonal antibody bound to the surfaces of Panc02, which constitutively expressed Neu5Gc, but Neu5Gc-preadsorbed anti-Neu5Gc polyclonal antibody could not react, indicating the anti-Neu5Gc antibody reacts to Neu5Gc specifically. Next, incorporation of Neu5Gc antigen via FBS-containing medium was examined (Fig. 1B). Fresh hADSCs/MSCs did not express Neu5Gc on their cell surface. In accordance with passage numbers, the population of Neu5Gc-positive cells has increased by cultivation with FBS (fresh: 0.33%; passage number 2: 19.77%; and passage number 5: 86.6%). Culture with heat-inactivated NHS could markedly reduce Neu5Gc in human colon carcinoma cells,[22] hESCs,[13] and hMSCs,[14] apparently as the result of metabolic replacement by *N*-acetylneuraminic acid in the human serum. So, the reduction of incorporated Neu5Gc xenoantigen by chasing cultivation with human serum was examined (Fig. 1C). The Neu5Gc xenoantigen was reduced after cultivation of hADSCs/MSCs with heat-inactivated NHS but not FBS. The percentages of Neu5Gc-positive cells have decreased in accordance with culture duration, and the decrement manners of second passaged hADSCs/MSCs and fifth passaged ones have been in a similar fashion.

Because human serum contains high titers of natural preformed antibodies against the Neu5Gc xenoantigen,[20–22] we assessed whether such antibodies could recognize Neu5Gc-containing epitopes on hADSCs/MSCs cultured with FBS (Fig. 2). Panc02 cultured with FBS and exposed to 10% fresh NHS containing 15 mM EDTA showed high human IgG (99.9%) and IgM (92.8%) binding (Fig. 2Aa). hADSCs/MSCs cultured with FBS and treated with fresh NHS also showed high human IgG binding (80.1%), but human IgM binding was very low (3.2%) (Fig. 2Ab). Preincubation of fresh NHS with Neu5Gc resulted in significant decrease in human IgG binding on hADSCs/MSCs cultured with FBS (80.1% to 2.08%). Further, pretreatment of hADSCs/MSCs with anti-Neu5Gc polyclonal antibody also resulted in reduction of human IgG binding (70.33% to 1.74%; Fig. 2B). Culturing hADSCs/MSCs with heat-inactivated NHS, which decreased Neu5Gc expression of hADSCs/MSCs effectively, reduced human IgG binding on hADSCs/MSCs when exposed to fresh NHS (Fig. 2C). Taken together, these data indicate that the hADSCs/MSCs cultured with FBS expressed Neu5Gc and the human natural preformed antibodies could bind to hADSCs/MSCs. This binding of human natural preformed antibodies on hADSCs/MSCs was related to the amount of Neu5Gc on hADSCs/MSCs. Culture with heat-inactivated NHS could markedly reduce IgG binding on hADSCs/MSCs when exposed to fresh NHS (80.1% to 3.9%).

Complement fragment deposition on hADSCs/MSCs and CMC assay

Cell surface antibody binding may activate the classical complement pathway leading to cytotoxicity. We assessed whether the deposition of complement fragments on hADSCs/MSCs occurred after exposure to fresh NHS. Whether hADSCs/MSCs were cultured with FBS or heat-inactivated NHS, the amount of deposition of C4 and C3 fragments on hADSCs/MSCs after a short incubation period of 30 min was no different from negative control (cells incubated with DMEM alone or 10% fresh NHS in DMEM containing 15 mM EDTA) (Fig. 3). To control for fresh NHS activity and variability, we tested the deposition of C4 and C3 fragments on Panc02. Both complement fragments were clearly deposited on Panc02 (C4: 84.6%; C3: 98.99%) and this deposition was abolished by adding 15% EDTA (Fig. 3). We next analyzed the CMC of hADSCs/MSCs cultured with FBS or heat-inactivated NHS. To control for CMC of fresh NHS,

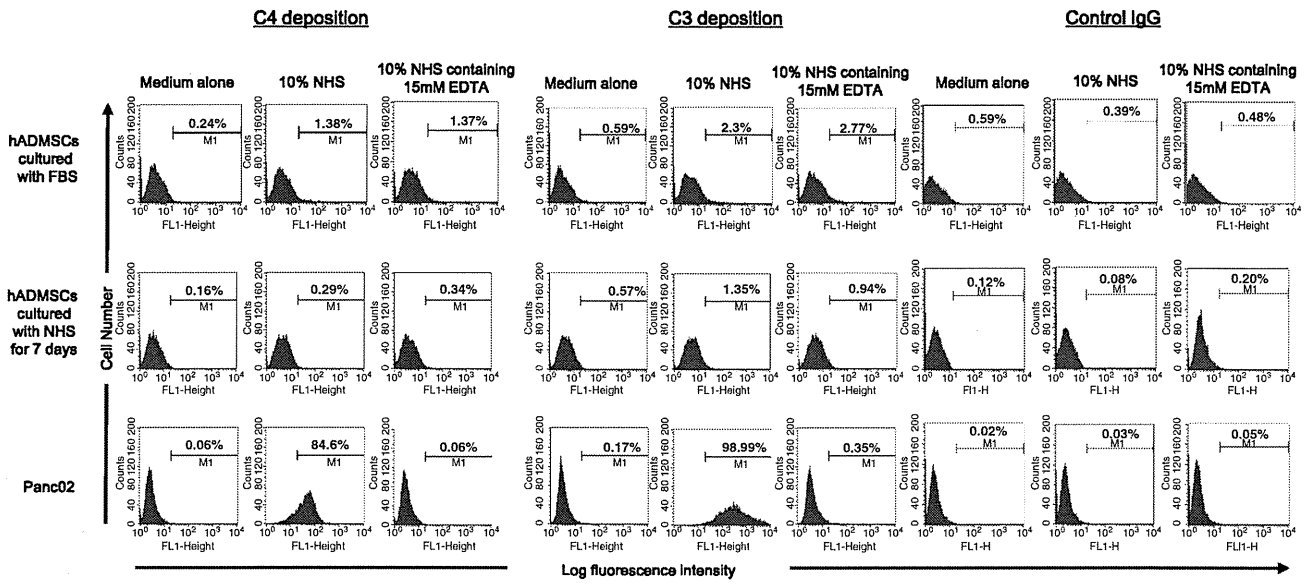

FIG. 3. Complement deposition onto hADSCs/MSCs by NHS. The cells were exposed to medium alone, 10% NHS, or 10% NHS containing 15 mM EDTA, followed by an analysis of deposition of complement fragments C4 and C3. The percentage of cells that stained positive is indicated in the upper right corner of each panel. Data are representative of four independent experiments.

we tested CMC of Panc02. CMC of Panc02 was clearly detected (20% NHS: 42.7% ± 4.7%; 40% NHS: 65.4% ± 2.4%). In contrast, significant specific lysis of hADSCs/MSCs cultured with FBS or heat-inactivated NHS was not detected (hADSCs/MSCs cultured with FBS + 20% NHS: 4.8% ± 1.3%; or 40% NHS: 7.4% ± 2.0%; hADSCs/MSCs cultured with heat-inactivated NHS: 20% NHS: 3.6% ± 1.6%; 40% NHS: 5.6% ± 1.6%). We then analyzed the expression of complement regulatory proteins such as CD46, CD55, and CD59 on hADSCs/MSCs. hADSCs/MSCs were weakly positive for both CD46 (22.1%) and CD55 (29.8%) and highly positive for CD59 (97.5%) (Fig. 4B). These data indicate that hADSCs/MSCs express complement regulatory proteins such as CD46, CD55, and CD59 and are largely resistant to killing by CMC mechanism.

ADCC of hADSCs/MSCs mediated by human natural preformed antibodies in NHS

IgG antibodies play an important role in ADCC.[28] Our study demonstrated that natural preformed IgG antibodies could bind to hADSCs/MSCs cultured with FBS. Therefore, to evaluate the role of these IgG antibodies in cell-mediated cytotoxicity, ADCC assay was performed with hADSCs/MSCs cultured with FBS, hADSCs/MSCs cultured with heat-inactivated NHS, or Panc02 as targets and human PBMCs as effector cells, using *E:T* ratios of 10:1 and 20:1, and 4-h incubation periods. PBMCs in the absence of heat-inactivated NHS caused no significant lysis of hADSCs/MSCs cultured with FBS, hADSCs/MSCs cultured with heat-inactivated NHS, and Panc02 (hADSCs/MSCs cultured with FBS: *E:T* = 10:1, 2.37% ± 0.35%; *E:T* = 20:1, 3.78% ± 0.85%; hADSCs/MSCs cultured with heat-inactivated NHS: *E:T* = 10:1, 0.57% ± 0.36%; *E:T* = 20:1, 2.34% ± 0.67%; Panc02: *E:T* = 10:1, 1.98% ± 0.35%; *E:T* = 20:1, 4.7% ± 0.54; Fig. 5, white bar). The cytotoxicity of Panc02 in the presence of heat-inactivated NHS was significantly greater than that in the absence of heat-inactivated NHS (in the presence of NHS vs. in the absence of heat-inactivated NHS: *E:T* = 10:1, 27.4% ± 3.1% vs. 1.98% ± 0.35%, $p < 0.05$; *E:T* = 20:1, 28.9% ± 4.6% vs. 4.7 ± 0.54%, $p < 0.05$), which proved the effective use of PBMCs (Fig. 5). A significant increase of cytotoxicity of the hADSCs/MSCs cultured with FBS was also evident in the presence of heat-inactivated NHS (in the presence of heat-inactivated NHS vs. in the absence of heat-inactivated NHS: *E:T* = 10:1, 13.5% ± 0.82% vs. 2.37% ± 0.35%, $p < 0.05$; *E:T* = 20:1, 16.0% ± 1.5% vs. 3.78% ± 0.85, $p < 0.05$; Fig. 5). In contrast, no increase of cytotoxicity of the hADSCs/MSCs cultured with heat-inactivated NHS was detected in the presence of heat-inactivated NHS (in the presence of heat-inactivated NHS vs. in the absence of heat-inactivated NHS: *E:T* = 10:1, 3.23% ± 0.52% vs. 0.57% ± 0.36%; *E:T* = 20:1, 3.75% ± 0.51% vs. 2.34% ± 0.67%; Fig. 5). In addition, the cytotoxicity the hADSCs/MSCs cultured with FBS was significantly greater than that of hADSCs/MSCs cultured with heat-inactivated NHS which expressed negligible amount of Neu5Gc (hADSCs/MSCs cultured with FBS vs. hADSCs/MSCs cultured with heat-inactivated NHS: *E:T* = 10:1, 13.5% ± 0.82% vs. 3.23% ± 0.52%, $p < 0.05$; *E:T* = 20:1, 16.0% ± 1.5% vs. 3.75% ± 0.51, $p < 0.05$; Fig. 5). Taken together, these data indicate that the hADSCs/MSCs cultured with FBS are injured by ADCC mechanism. In contrast, hADSCs/MSCs cultured with NHS are less sensitive to ADCC.

Phagocytosis of hADSCs/MSCs by human monocyte-derived macrophages

hADSCs/MSCs cultured with FBS, hADSCs/MSCs cultured with heat-inactivated NHS, or Panc02 were stained with fluorescent PKH67, respectively. Labeled cells were cocultured with human monocyte-derived macrophages in the presence or absence of heat-inactivated NHS for 24 h. After counterstaining with monoclonal antibodies to human CD11c, two-color flow cytometric analysis was performed

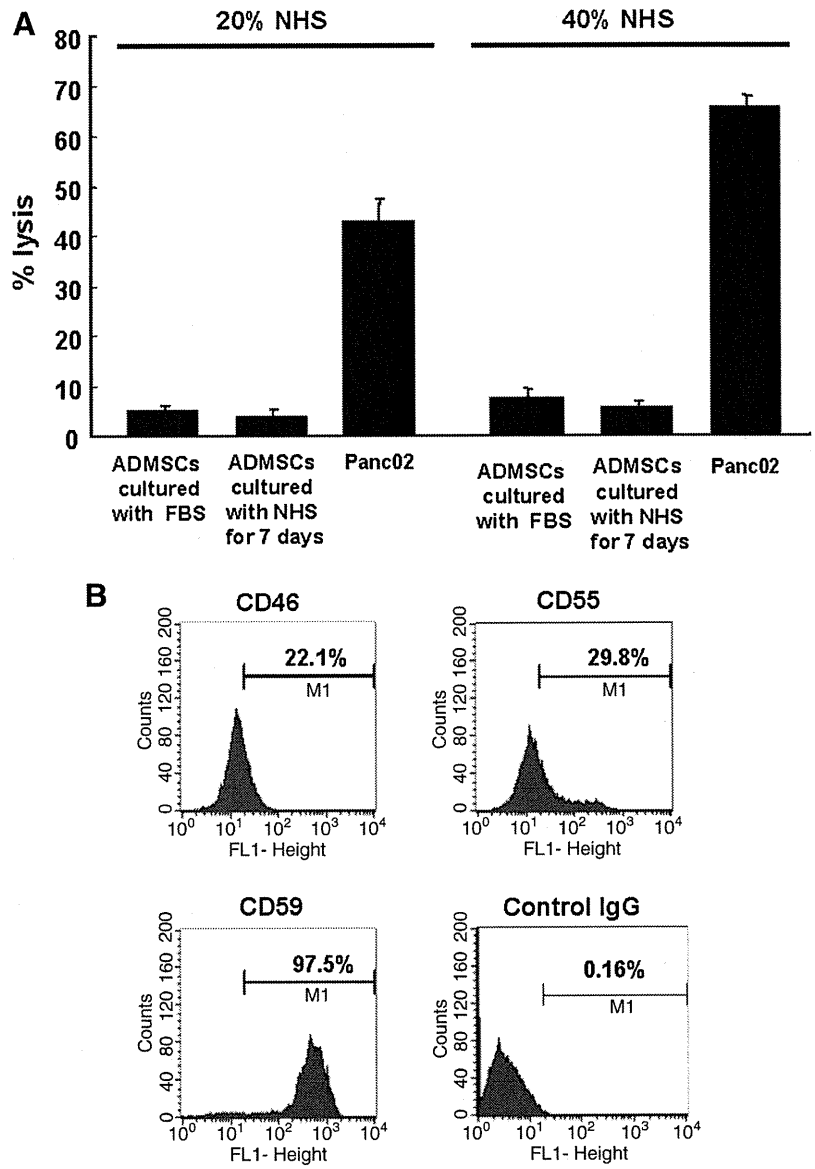

FIG. 4. Sensitivity of hADMSCs to lysis by NHS. (**A**) Complement-mediated cytotoxicity assay of hADSCs/MSCs. The cytotoxic activity of 20% or 40% NHS against hADSCs/MSCs was tested by lactate dehydrogenase release. Data are shown as mean ± standard deviation. (**B**) Complement regulatory proteins on hADSCs/MSCs were studied by flow cytometry using FITC-conjugated antibodies to human CD46, CD55, CD59, or control IgG. Data are representative of three independent experiments.

(Fig. 6). Phagocytosis of target cells by human monocyte-derived macrophages could be identified as dual-labeled cells ($PKH67^+/CD11c^+$, right upper panel). Similar results were obtained in three independent experiments. Phagocytosis of Panc02 was clearly detectable (10.6%) and increased twofold in the presence of heat-inactivated NHS, which proved the effective use of human monocyte-derived macrophages. Phagocytosis of hADSCs/MSCs cultured with NHS by human monocyte-derived macrophages was somewhat detectable (5.7%) and also increased in the presence of heat inactivated human serum (9.3%). In contrast, human monocyte-derived macrophages could not phagocytose hADSCs/MSCs cultured with heat-inactivated NHS neither in the absence nor in the presence of heat-inactivated NHS (medium alone: 1.1%; 10% heat-inactivated NHS: 2.2%; Fig. 6). Thus, human monocyte-derived macrophages phagocytosed hADSCs/MSCs cultured with FBS and this phagocytic activity increased when hADSCs/MSCs cultured with FBS were opsonized by the natural preformed antibodies in the presence of heat-inactivated NHS. In contrast, hADSCs/MSCs cultured with heat-inactivated NHS were resistant to phagocytosis either in the absence or in the presence of heat-inactivated NHS.

Adipogenic and osteogenic differentiation potentials of hADSCs/MSCs cultured with FBS and heat-inactivated NHS

To compare the *in vitro* differentiation potential of hADSCs/MSCs cultured with FBS or heat-inactivated NHS, cells were differentiated toward the adipogenic and osteogenic lineages. Adipogenic differentiation was induced by culture with differentiation medium containing 1-methyl-3-isobutylxanthine, peroxisome proliferator-activated receptor (PPAR)-gamma agonist, dexamethasone, and insulin. The acquisition of the adipogenic phenotype was determined by staining the cell monolayers with oil red O (Fig. 7A). The efficiency of adipogenesis of hADSCs/MSCs cultured with heat-inactivated NHS was similar to that of hADSCs/MSCs cultured with FBS (Fig. 7A). Both hADSCs/MSCs showed multiple intracellular lipid-

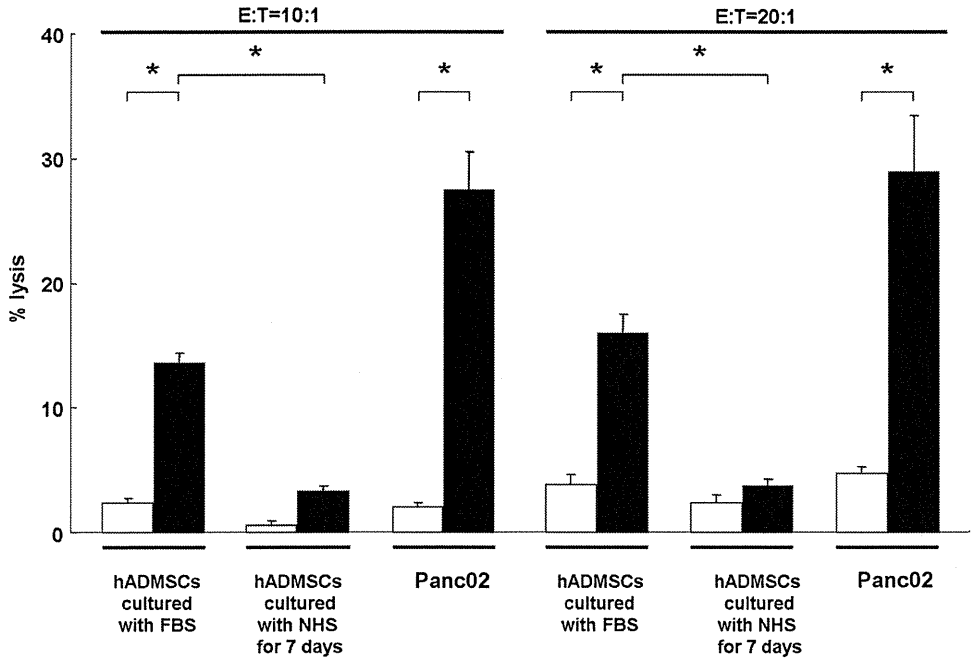

FIG. 5. Antibody-dependent cell-mediated cytotoxicity assay of hADSCs/MSCs. The cytotoxic activity of peripheral blood mononuclear cells against hADSCs/MSCs in the absence (white bar) or presence (black bar) of 10% NHS was tested by measuring lactate dehydrogenase release into medium (Effector:Target [*E:T*] = 10:1 or 20:1). Data are shown as mean ± standard deviation ($*p < 0.05$) and are representative of three independent experiments.

filled droplets in 35–50% of cells after adipogenic induction. Osteogenic differentiation was induced by treating cells with low concentrations of dexamethasone, ascorbic acid, and beta-glycerophosphate. Calcium deposition was demonstrated by staining monolayers with alizarin red (Fig. 7B). hADSCs/MSCs cultured with heat-inactivated NHS and those cultured with FBS showed similar potential toward osteogenic differentiation. High AP activity was detected in hADSCs/MSCs cultured with heat-inactivated NHS and those cultured with FBS in response to osteogenic induction after 2 weeks (Fig. 7B).

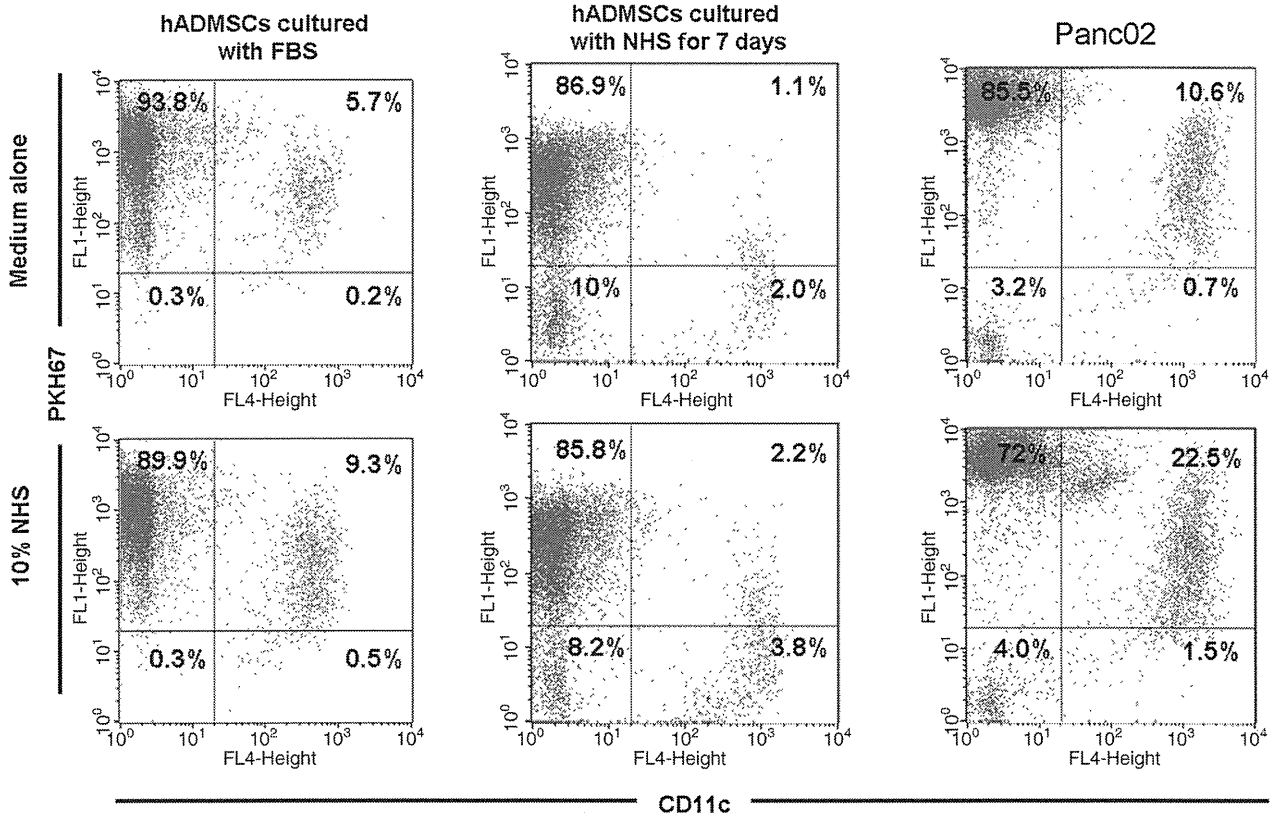

FIG. 6. Representative flow cytometry profiles of phagocytosis assay of hADSCs/MSCs. Upper left quadrant: Region of residual target cells. Upper right quadrant: Region of phagocytosed target cells. Percentages represent those of total cells in each region. Data are representative of three independent experiments.

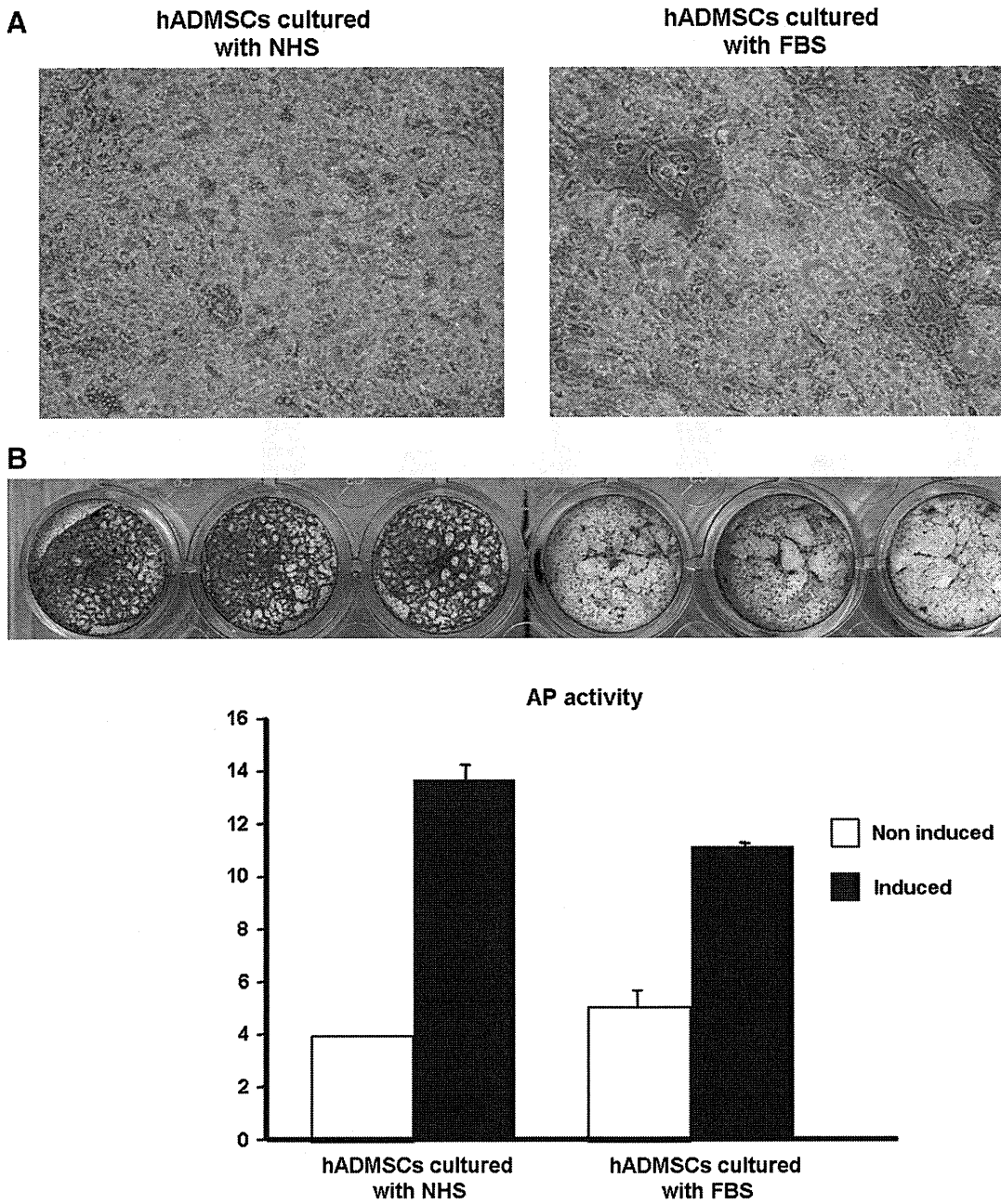

FIG. 7. Adipogenic and osteogenic differentiation potentials of hADSCs/MSCs cultured with FBS and NHS. (**A**) The efficiency of adipogenesis of hADSCs/MSCs cultured with NHS was similar to that of hADSCs/MSCs cultured with FBS. (**B**) The efficacy of osteogenic differentiation and alkaline phosphatase activity was similar between cultures with NHS and FBS in response to osteogenic induction. Data are representative of four independent experiments.

Discussion

Previous studies have reported that hESCs and BM-derived hMSCs are capable of efficient Neu5Gc uptake from culture media components.[13,14] Human serum contains high titers of natural preformed antibodies against Neu5Gc xenoantigen[20–22] and binding of these natural preformed antibodies may lead to immune responses. Importantly, this may be reflected in the published results of human clinical trials using BM-derived hMSCs cultured with FBS.[8–12] Further, in human clinical trials with FBS-grown hMSCs, antibodies against FBS have been detected.[12] However, these immune responses against human stem cells mediated by natural preformed antibodies remain in controversary.[13,23] In this study, because of the usefulness of hADSCs/MSCs as an alternative source of stem cells, we assessed the presence of Neu5Gc in hADSCs/MSCs cultured with FBS and the human immune response mediated by Neu5Gc xenoantigen.

Our study using a chicken anti-Neu5Gc polyclonal antibody showed that most of the hADSCs/MSCs cultured with FBS expressed Neu5Gc xenoantigen. This result is similar to the previous study that hESCs and BM-derived hMSCs express Neu5Gc.[13,14] In addition, our data suggested

that human natural preformed antibodies could bind to hADSCs/MSCs after exposure to fresh NHS. The subtype of natural preformed antibodies was mainly IgG, not IgM. This human IgG binding was related to the amount of Neu5Gc on the hADSCs/MSCs, because hADSCs/MSCs cultured with heat-inactivated NHS which expressed negligible levels of Neu5Gc showed negligible levels of IgG binding when exposed to fresh NHS. This result is also consistent with the previous study that anti-Neu5Gc antibodies constitute the majority of natural preformed xenoreactive antibodies besides anti-galactose-alpha 1,3-galactose (Gal) antibodies, particularly in the IgG subclass.[20,29] In effect, hADSCs/MSCs cultured with FBS may seem like xenogeneic cells to the human immune systems.

When xenogeneic grafts are transplanted into humans, binding of natural preformed antibodies that recognize xenoantigens, including Gal and Neu5Gc, mediates two types of rejection response, hyperacute rejection (HAR) and acute humoral xenograft rejection (AHXR).[30] HAR begins with binding of natural preformed antibodies to the xenogeneic epitopes on donor endothelial cells, including Gal and Neu5Gc xenoantigens, leading to complement activation by mainly classical pathway.[30] The graft is rejected within minutes to hours. Therefore, we analyzed the CMC of hADSCs/MSCs cultured with FBS that express Neu5Gc xenoantigen, using fresh NHS. However, we could not confirm the existence of CMC. The deposition of C4 and C3 fragments on hADSCs/MSCs after a short incubation with fresh NHS could not also be detected. In this issue, there are no reports describing the CMC of hADSCs/MSCs cultured with FBS that express Neu5Gc xenoantigen. Martin *et al.* reported that binding of natural preformed antibodies to Neu5Gc on hESCs mediated complement activation leading to cell death.[13] In contrast, Cerdan *et al.* reported that complement activation by anti-Neu5Gc antibody does not mediate killing of hESCs.[23] Several reasons for this discrepancy have been supposed. One is the difference of procedures used for testing cell cytotoxicity. Previous two reports detected cell cytotoxicity by propidium iodide or 7-AAD exclusion using flow cytometry. Single-cell suspension required for this procedure may cause extensive cell death even under controlled conditions. We detected cell cytotoxicity by conventional LDH release assay, which is often used in cytotoxicity assays.[32,33] The other and more possible reason is the biological difference among the human stem cells, including hESCs and hMSCs. We assessed the expression of complement regulatory proteins such as CD46, CD55, and CD59 on hADSCs/MSCs. hADSCs/MSCs were weakly positive for both CD46 and CD55 and highly positive for CD59. It is reported that HAR could be prevented by inhibiting complement activation, using transgenic animals bearing transgenes encoding human complement regulatory proteins.[34–36] Thus, it is supported that hADSCs/MSCs express complement regulatory proteins and may be largely resistant to killing by CMC mechanism. However, the expression of complement regulatory proteins on other human stem cells such as hESCs remains uncertain and further investigation is needed.

AHXR occurs when HAR is prevented, and it can be induced by low levels of natural preformed antibodies.[30] The binding of natural preformed antibodies to xenogeneic endothelial cells results in ADCC by natural killer cells, macrophages, and neutrophils, endothelial cell activation, thrombosis, and vasoconstriction.[30] It is reported that AHXR could be mediated by natural preformed antibodies against non-Gal xenoantigen,[37,38] particularly Neu5Gc xenoantigen.[39] Therefore, we analyzed the ADCC of hADSCs/MSCs cultured with FBS that express Neu5Gc xenoantigen. Our data indicated the clear existence of ADCC of hADSCs/MSCs cultured with FBS. This ADCC is supposed to be mediated by preformed natural antibodies that recognize Neu5Gc because ADCC of hADSCs/MSCs cultured with heat-inactivated NHS which expressed negligible levels of Neu5Gc could not be detected. We also analyzed the antibody-mediated cell phagocytosis of hADSCs/MSCs cultured with FBS by monocyte-derived macrophage because macrophages can target opsonized cells. However, in our study, a low level of phagocytic activity of hADSCs/MSCs cultured with FBS even in the absence of NHS was detected and this phagocytic activity clearly increased in the presence of NHS. Ide *et al.* reported that human macrophages could phagocytose porcine cells in an antibody- and complement-independent manner and elimination of Gal on porcine cells that expressed Neu5Gc did not prevent this phagocytic activity.[40] Our data indicated that hADSCs/MSCs cultured with heat-inactivated NHS which expressed negligible levels of Neu5Gc were resistant to phagocytosis mediated by human macrophages in the presence or absence of fresh NHS. Accordingly, human macrophages may be able to recognize Neu5Gc xenoantigen and phagocytose hADSCs/MSCs.

We showed here that hADSCs/MSCs cultured with FBS expressed Neu5Gc xenoantigen and that binding of natural preformed antibodies led to immune response. Based on current data, it is clear that hADSCs/MSCs should be chased without animal materials. Yamaguchi *et al.* have tried xeno-free techniques on hematopoietic stem cells by growing them on human stromal cells and using medium containing NHS.[41] To eliminate Neu5Gc on hADSCs/MSCs, we cultured them in a medium in which FBS was replaced by heat-inactivated NHS for a week after culturing with FBS. The expression of Neu5Gc on these hADSCs/MSCs was extremely reduced. Heiskanen *et al.* described that BM-derived hMSCs became decontaminated after 2 weeks of culture in a medium in which FBS was replaced by NHS, but complete decontamination was difficult to achieve by changing culture conditions.[14] Therefore, hADSCs/MSCs may not be completely decontaminated with Neu5Gc by culturing with heat-inactivated NHS for a week. However, our data suggested that human immune responses mediated by Neu5Gc on hADSCs/MSCs, such as ADCC and phagocytosis, were nearly completely prevented by this culture condition. Adipogenic and osteogenic differentiation potentials of hADSCs/MSCs cultured with heat-inactivated NHS were not less than that of those cultured with FBS. This work implies that the culture conditions avoiding renewed exposure to animal materials can reduce the expression of Neu5Gc on hADSCs/MSCs and consequently prevent human immune responses against hADSCs/MSCs. Although major complications have not been reported in the clinical trials with hMSCs cultured with FBS, human immune responses mediated by Neu5Gc may potentially influence the survival and efficacy of the transplanted cells and thus bias the published results. For clinical application of stem cell therapies based on hADSCs/MSCs, hADSCs/MSCs that presented Neu5Gc on their cell surfaces after

exposure to FBS should be cleaned up by chasing without Neu5Gc condition and thus might be rescued from xenogeneic rejection.

Acknowledgments

The authors thank Prof. Nobutaka Wakamiya, Department of Microbiology and Immunochemistry, Asahikawa Medical College, Hokkaido, Japan, for providing a chicken anti-Neu5Gc polyclonal antibody. This study was supported in part by a grant-in-aid to Akifumi Matsuyama from the Kobe Translational Research Cluster, the Knowledge Cluster Initiative, Ministry of Education, Culture, Sports, Science, and Technology (MEXT), Japan, and by the Program for Promotion of Fundamental Studies in Health Sciences of the National Institute of Biomedical Innovation (NIBIO), Japan.

Disclosure Statement

No competing financial interests exist.

References

1. Björntorp, P., Karlsson, M., Gustafsson, L., Smith, U., Sjöström, L., Cigolini, M., Storck, G., and Pettersson, P. Quantitation of different cells in the epididymal fat pad of the rat. J Lipid Res **20,** 97, 1979.
2. Zuk, P.A., Zhu, M., Ashjian, P., De Ugarte, D.A., Huang, J.I., Mizuno, H., Alfonso, Z.C., Fraser, J.K., Benhaim, P., and Hedrick, M.H. Human adipose tissue is a source of multipotent stem cells. Mol Biol Cell **13,** 4279, 2002.
3. Okura, H., Matsuyama, A., Lee, C.M., Saga, A., Kakuta-Yamamoto, A., Nagao, A., Sougawa, N., Sekiya, N., Takekita, K., Shudo, Y., Miyagawa, S., Komoda, H., Okano, T., and Sawa, Y. Cardiomyoblast-like cells differentiated from human adipose tissue-derived mesenchymal stem cells improve left ventricular dysfunction and survival in a rat myocardial infarction model. Tissue Eng Part C Methods July 22, 2009. [Epub ahead of print].
4. Okura, H., Fumimoto, Y., Komoda, H., Yanagisawa, T., Nishida, T., Noguchi, S., Sawa, Y., and Matsuyam, A. Transdifferentiation of human adipose tissue-derived stromal cells into insulin-producing clusters. J Artif Organs **12,** 123, 2009.
5. Pittenger, M.F., Mackay, A.M., Beck, S.C., Jaiswal, R.K., Douglas, R., Mosca, J.D., Moorman, M.A., Simonetti, D.W., Craig, S., and Marshak, D.R. Multilineage potential of adult human mesenchymal stem cells. Science **284,** 143, 1999.
6. Kern, S., Eichler, H., Stoeve, J., Klüter, H., Bieback, K. Comparative analysis of mesenchymal stem cells from bone marrow, umbilical cord blood, or adipose tissue. Stem Cells **24,** 1294, 2006.
7. Romanov, Y.A., Darevskaya, A.N., Merzlikina, N.V., and Buravkova, L.B. Mesenchymal stem cells from human bone marrow and adipose tissue: isolation, characterization, and differentiation potentialities. Bull Exp Biol Med **140,** 138, 2005.
8. Sotiropoulou, P.A., Perez, S.A., Salagianni, M., Baxevanis, C.N., and Papamichail, M. Characterization of the optimal culture conditions for clinical scale production of human mesenchymal stem cells. Stem Cells **24,** 462, 2006.
9. Mazzini, L., Fagioli, F., Boccaletti, R., Mareschi, K., Oliveri, G., Olivieri, C., Pastore, I., Marasso, R., and Madon, E. Stem cell therapy in amyotrophic lateral sclerosis: a methodological approach in humans. Amyotroph Lateral Scler Other Motor Neuron Disord **4,** 158, 2003.
10. Bang, O.Y., Lee, J.S., Lee, P.H., and Lee, G. Autologous mesenchymal stem cell transplantation in stroke patients. Ann Neurol **57,** 874, 2005.
11. Chen, S.L., Fang, W.W., Ye, F., Liu, Y.H., Qian, J., Shan, S.J., Zhang, J.J., Chunhua, R.Z., Liao, L.M., Lin, S., and Sun, J.P. Effect on left ventricular function of intracoronary transplantation of autologous bone marrow mesenchymal stem cell in patients with acute myocardial infarction. Am J Cardiol **94,** 92, 2004.
12. Horwitz, E.M., Gordon, P.L., Koo, W.K., Marx, J.C., Neel, M.D., McNall, R.Y., Muul, L., and Hofmann, T. Isolated allogeneic bone marrow-derived mesenchymal cells engraft and stimulate growth in children with osteogenesis imperfecta: implications for cell therapy of bone. Proc Natl Acad Sci USA **99,** 8932, 2002.
13. Martin, M.J., Muotri, A., Gage, F., and Varki, A. Human embryonic stem cells express an immunogenic nonhuman sialic acid. Nat Med **11,** 228, 2005.
14. Heiskanen, A., Satomaa, T., Tiitinen, S., Laitinen, A., Mannelin, S., Impola, U., Mikkola, M., Olsson, C., Miller-Podraza, H., Blomqvist, M., Olonen, A., Salo, H., Lehenkari, P., Tuuri, T., Otonkoski, T., Natunen, J., Saarinen, J., and Laine, J. *N*-Glycolylneuraminic acid xenoantigen contamination of human embryonic and mesenchymal stem cells is substantially reversible. Stem Cells **25,** 197, 2007.
15. Nowak, J.A., Jain, N.K., Stinson, M.W., and Merrick, J.M. Interaction of bovine erythrocyte *N*-glycolylneuraminic acid-containing gangliosides and glycoproteins with a human Hanganutziu-Deicher serum. Mol Immunol **23,** 693, 1986.
16. Chou, H.H., Takematsu, H., Diaz, S., Iber, J., Nickerson, E., Wright, K.L., Muchmore, E.A., Nelson, D.L., Warren, S.T., and Varki, A. A mutation in human CMP-sialic acid hydroxylase occurred after the Homo-Pan divergence. Proc Natl Acad Sci USA **95,** 11751, 1998.
17. Hayakawa, T., Satta, Y., Gagneux, P., Varki, A., and Takahata, N. *Alu*-mediated inactivation of the human CMP-*N*-acetylneuraminic acid hydroxylase gene. Proc Natl Acad Sci USA **98,** 11399, 2001.
18. Bardor, M., Nguyen, D.H., Diaz, S., and Varki, A. Mechanism of uptake and incorporation of the non-human sialic acid *N*-glycolylneuraminic acid into human cells. J Biol Chem **280,** 4228, 2005.
19. Lanctot, P.M., Gage, F.H., and Varki, A.P. The glycans of stem cells. Curr Opin Chem Biol **11,** 373, 2007.
20. Zhu, A., and Hurst, R. Anti-*N*-glycolylneuraminic acid antibodies identified in healthy human serum. Xenotransplantation **9,** 376, 2002.
21. Nguyen, D.H., Tangvoranuntakul, P., and Varki, A. Effects of natural human antibodies against a nonhuman sialic acid that metabolically incorporates into activated and malignant immune cells. J Immunol **175,** 228, 2005.
22. Tangvoranuntakul, P., Gagneux, P., Diaz, S., Bardor, M., Varki, N., Varki, A., and Muchmore, E. Human uptake and incorporation of an immunogenic nonhuman dietary sialic acid. Proc Natl Acad Sci USA **100,** 12045, 2003.
23. Cerdan, C., Bendall, S.C., Wang, L., Stewart, M., Werbowetski, T., and Bhatia, M. Complement targeting of nonhuman sialic acid does not mediate cell death of human embryonic stem cells. Nat Med **12,** 1113, 2006.
24. Asaoka, H., Nishinaka, S., Wakamiya, N., Matsuda, H., and Murata, M. Two chicken monoclonal antibodies specific for

heterophil Hanganutziu-Deicher antigens. Immunol Lett **32,** 91, 1992.
25. Matsuyama, A., Yamashita, S., Sakai, N., Maruyama, T., Okuda, E., Hirano, K., Kihara, S., Hiraoka, H., and Matsuzawa, Y. Identification of a GPI-anchored type HDL-binding protein on human macrophages. Biochem Biophys Res Commun **272,** 864, 2000.
26. Hashikawa, T., Takedachi, M., Terakura, M., Yamada, S., Thompson, L.F., Shimabukuro, Y., and Murakami, S. Activation of adenosine receptor on gingival fibroblasts. J Dent Res **85,** 739, 2006.
27. Labarca, C., and Paigen, K. A simple, rapid, and sensitive DNA assay procedure. Anal Biochem **102,** 344, 1980.
28. Schaapherder, A.F., Daha, M.R., te Bulte, M.T., van der Woude, F.J., and Gooszen, H.G. Antibody-dependent cell-mediated cytotoxicity against porcine endothelium induced by a majority of human sera. Transplantation **57,** 1376, 1994.
29. Ezzelarab, M., Ayares, D., and Cooper, D.K. Carbohydrates in xenotransplantation. Immunol Cell Biol **83,** 396, 2005.
30. Yang, Y.G., and Sykes, M. Xenotransplantation: current status and a perspective on the future. Nat Rev Immunol **7,** 519, 2007.
31. Roos, A., and Daha, M.R. Antibody-mediated activation of the classical complement pathway in xenograft rejection. Transpl Immunol **9,** 257, 2002.
32. Miyagawa, S., Kubo, T., Matsunami, K., Kusama, T., Beppu, K., Nozaki, H., Moritan, T., Ahn, C., Kim, J.Y., Fukuta, D., and Shirakura, R. Delta-short consensus repeat 4-decay accelerating factor (DAF: CD55) inhibits complement-mediated cytolysis but not NK cell-mediated cytolysis. J Immunol **173,** 3945, 2004.
33. Komoda, H., Miyagawa, S., Kubo, T., Kitano, E., Kitamura, H., Omori, T., Ito, T., Matsuda, H., and Shirakura, R. A study of the xenoantigenicity of adult pig islets cells. Xenotransplantation **11,** 237, 2004.
34. Diamond, L.E., Quinn, C.M., Martin, M.J., Lawson, J., Platt, J.L., and Logan, J.S. A human CD46 transgenic pig model system for the study of discordant xenotransplantation. Transplantation **71,** 132, 2001.
35. Schuurman, H.J., Pino-Chavez, G., Phillips, M.J., Thomas, L., White, D.J., and Cozzi, E. Incidence of hyperacute rejection in pig-to-primate transplantation using organs from hDAF-transgenic donors. Transplantation **73,** 1146, 2002.
36. Zhou, C.Y., McInnes, E., Copeman, L., Langford, G., Parsons, N., Lancaster, R., Richards, A., Carrington, C., and Thompson, S. Transgenic pigs expressing human CD59, in combination with human membrane cofactor protein and human decay-accelerating factor. Xenotransplantation **12,** 142, 2005.
37. Chen, G., Qian, H., Starzl, T., Sun, H., Garcia, B., Wang, X., Wise, Y., Liu, Y., Xiang, Y., Copeman, L., Liu, W., Jevnikar, A., Wall, W., Cooper, D.K., Murase, N., Dai, Y., Wang, W., Xiong, Y., White, D.J., and Zhong, R. Acute rejection is associated with antibodies to non-Gal antigens in baboons using Gal-knockout pig kidneys. Nat Med **11,** 1295, 2005.
38. Chen, G., Sun, H., Yang, H., Kubelik, D., Garcia, B., Luo, Y., Xiang, Y., Qian, A., Copeman, L., Liu, W., Cardella, C.J., Wang, W., Xiong, Y., Wall, W., White, D.J., and Zhong, R. The role of anti-non-Gal antibodies in the development of acute humoral xenograft rejection of hDAF transgenic porcine kidneys in baboons receiving anti-Gal antibody neutralization therapy. Transplantation **81,** 273, 2006.
39. Saethre, M., Baumann, B.C., Fung, M., Seebach, J.D., and Mollnes, T.E. Characterization of natural human anti-non-gal antibodies and their effect on activation of porcine gal-deficient endothelial cells. Transplantation **84,** 244, 2007.
40. Ide, K., Ohdan, H., Kobayashi, T., Hara, H., Ishiyama, K., and Asahara, T. Antibody- and complement-independent phagocytotic and cytolytic activities of human macrophages toward porcine cells. Xenotransplantation **12,** 181, 2005.
41. Yamaguchi, M., Hirayama, F., Wakamoto, S., Fujihara, M., Murahashi, H., Sato, N., Ikebuchi, K., Sawada, K., Koike, T., Kuwabara, M., Azuma, H., and Ikeda, H. Bone marrow stromal cells prepared using AB serum and bFGF for hematopoietic stem cells expansion. Transfusion **42,** 921, 2002.

Address correspondence to:
Akifumi Matsuyama, M.D., Ph.D.
Department of Somatic Stem Cell Therapy
Institute of Biomedical Research and Innovation
Foundation for Biomedical Research and Innovation
1-5-4 TRI 305
Minatojima-Minamimachi
Chuo-ku
Kobe 650-0047
Japan

E-mail: akifumi-matsuyama@umin.ac.jp

Received: June 9, 2009
Accepted: October 27, 2009
Online Publication Date: December 18, 2009

ORAL DISEASES

Oral Diseases (2010) 16, 812–817. doi:10.1111/j.1601-0825.2010.01693.x
© 2010 John Wiley & Sons A/S
All rights reserved
www.wiley.com

ORIGINAL ARTICLE

Suppressive effects of nicotine on the cytodifferentiation of murine periodontal ligament cells

M Yanagita, Y Kojima, T Kawahara, T Kajikawa, H Oohara, M Takedachi, S Yamada, S Murakami

Department of Periodontology, Division of Oral Biology and Disease Control, Osaka University Graduate School of Dentistry, Osaka, Japan

OBJECTIVES: Tobacco smoking has been suggested to be one of the important risk factors of developing periodontal disease. Although epidemiological studies have shown the detrimental effects of smoking on periodontal disease, the effects of smoke compounds on gingival tissue are not well understood. The aim of this study was to evaluate the effects of nicotine, which is the major component of the thousands of chemicals that constitute cigarette smoke, for cytodifferentiation of murine periodontal ligament (MPDL) cell.

MATERIALS AND METHODS: Expression of nAChR subunits on MPDL cells was examined using RT-PCR. The effects of nicotine on gene expression of extracellular matrices and osteoblastic transcription factors were evaluated by quantitative RT-PCR. Mineralized nodule formation of nicotine-treated MPDL cells was characterized by alizarin red staining.

RESULTS: Murine periodontal ligament cells expressed several subunits of nAChR, which have functional calcium signals in response to nicotine. Gene expression of extracellular matrices and osteoblastic transcription factors were reduced in nicotine-treated MPDL cells. In addition, mineralized nodule formation was inhibited in MPDL cells in the presence of nicotine.

CONCLUSION: Our findings indicate that nicotine may negatively regulate the cytodifferentiation and mineralization of MPDL cells.

Oral Diseases (2010) **16**, 812–817

Keywords: periodontal ligament cells; nicotine; cytodifferentiation; mineralization

Introduction

The periodontal ligament (PDL) is a connective tissue that surrounds the root of the tooth and attaches the root to the alveolar bone to provide mechanical support. The PDL also plays a nutritive and sensory role. In addition, PDL is regarded as a reservoir of multipotential mesenchymal stem cells that can differentiate into mineralized tissue-forming cells, such as osteoblasts and cementoblasts (Seo *et al*, 2004), and plays an important role in periodontal tissue remodeling and regeneration.

Cigarette smoking is known to be one of the most important risk factors in periodontal disease (Martinez-Canut *et al*, 1996; Ryder, 2007). Previous reports have shown that more clinical attachment loss and alveolar bone loss have been observed in smokers than in non-smokers (Grossi *et al*, 1994; Grossi *et al*, 1995). Tobacco smoke consists of thousands of chemicals (Lofroth, 1989) which individually, and collectively, can affect periodontal tissue. Nicotine is the main component of tobacco smoke and a selective agonist of the nicotinic acetylcholine receptor (nAChR). The main route of nicotine exposure is via inhalation of tobacco smoke. During inhalation, a high dose of nicotine (in excess of 10^{-3} M) would be exposed to the epithelial surface of the oral cavity, the bronchus and the lungs (Feyerabend *et al*, 1982; Seow *et al*, 1994). In particular, nicotine concentrations in the saliva of long-term snuff users can reach 9.6 mM (Hoffmann and Adams, 1981; Sato *et al*, 2008).

Therefore, we hypothesized that nicotine affects the characteristics of PDL directly and has detrimental effects on periodontal tissue, such as disease progression and the ineffectiveness for periodontal treatment. In this study, we investigated the gene expression of nAChR subunits and calcium influx via these receptors using a PDL clone obtained from murine PDL (MPDL) tissue (Yamada *et al*, 2007). We then examined the gene expression of alkaline phosphatase (ALP), collagen type I, bone sialoprotein (BSP), osterix, and runx2 in nicotine-treated MPDL. Further, the effects of nicotine on mineralization in MPDL were evaluated.

Materials and methods

Culture of MPDL

We have established a murine PDL clone cell, MPDL22, isolated from the PDL tissue of the molar teeth extracted from 2.5-week-old BALB/c mice (Yamada

Correspondence: Dr S Murakami, Department of Periodontology, Division of Oral Biology and Disease Control, Osaka University Graduate School of Dentistry, 1-8 Yamadaoka, Suita, Osaka 565-0871, Japan. Tel: +81 6 6879 2930, Fax: +81 6 6879 2934, E-mail: ipshinya@dent.osaka-u.ac.jp
Received 3 January 2010; revised 7 February 2010; accepted 17 February 2010

et al, 2007). MPDL22 cells were maintained in α-MEM (Nikken, Kyoto, Japan) supplemented with 10% fetal calf serum (FCS; JRH Biosciences, Lenexa, KS, USA) and 100 ng ml^{-1} fibroblast growth factor-2 (FGF-2; Kaken, Kyoto, Japan) at 37°C in a humidified atmosphere of 5% CO^2. After the cells reached confluence, we replaced the culture medium (α-MEM supplemented with 10% FCS and FGF-2) with the mineralization medium (α-MEM supplemented with 10% FCS, 10 mM β-glycerophosphate, and 50 μg ml^{-1} ascorbic acid). We replaced the mineralization medium every 2 days with or without nicotine (10^{-8} M to 10^{-3} M), which was prepared in PBS and neutralized to pH 7.2.

Detection of nAChRs in MPDL by RT-PCR
MPDL22 cells were seeded at a density of 10^5 cells per dish in 60 mm dishes and grown to confluency. Following the culture of MPDL cells, total RNA was extracted using the RNAbee (TEL-TEST, Friendswood, TX, USA), according to the manufacturer's instructions. cDNA synthesis and amplification via PCR were performed, as described previously (Yamada *et al*, 2007). The primers used for PCR were prepared according to published results (Kageyama-Yahara *et al*, 2008). After denaturation at 94°C for 5 min, each PCR cycle consisted of 94°C for 30 s, 60°C for 45 s and 68°C for 45 s. Amplified products were analyzed by electrophoresis at 100 V for 30 min on 1.5% TAE agarose gels containing 0.5 μg ml^{-1} ethidium bromide. Murine brain samples were used as a positive control for nAChR subunits.

RT-PCR for ALP, collagen type I, BSP, osterix and runx2 mRNA
RNA samples were obtained from MPDL22 cells in α-MEM containing 1% FCS 2 days after nicotine treatment (10^{-3} M). Total RNA extract (0.4 mg) was reverse-transcribed using the High Capacity cDNA Reverse Transcriptase kit (Applied Biosystems, Foster City, CA, USA) to generate the single-stranded cDNA. PCRs were carried out using the ABI 7300 Fast Real-Time PCR System (Applied Biosystems) with Power SYBR^R Green PCR Master Mix (Applied Biosystems) according to the manufacturer's protocol. All reactions were run in triplicate. The primer sequences used for RT-PCR were as follows; ALP, (sense) 5′-ACA CCT GAC TGT GGT TAC TGC TGA-3′, (antisense) 5′-CCT TGT AGC CAG GCC CGT TA-3′; collagen type I, (sense) 5′-ATG CCG CGA CCT CAA GAT G-3′, (antisense) 5′-TGA GGC ACA GAC GGC TGA GTA-3′; BSP, (sense) 5′-TGG AGA CTG CGA TAG TTC CGA AG-3′, (antisense) 5′-CGT AGC TAG CTG TTA CAC CCG AGA G-3′; Osterix, (sense) 5′-CGC ATC TGA AAG CCC ACT TG-3′, (antisense) 5′-CAG CTC GTC AGA GCG AGT GAA-3′; runx2, (sense) 5′-CAC TGG CGG TGC AAC AAG A-3′, (antisense) 5′-TTT CAT AAC AGC GGA GGC ATT TC-3′.

Proliferation assay
MPDL22 (5×10^3 cells per well) were incubated in 96-well plates in α-MEM containing 1% FCS in the presence of nicotine or FGF-2 (100 ng ml^{-1}) for 48 h. Cell proliferation was measured using the non-radioactive colorimetric assay WST-1 system (Roche Diagnostics GmbH, Penzberg, Germany) according to the manufacturer's instructions and the OD450/650 measured after 2 h on a microplate reader (Bio-Rad, Hercules, CA, USA).

Intracellular calcium determination
The cells (2×10^4 cells per well) were incubated onto 96-well plates for 24 h and washed in PBS containing 1 mM Ca^{2+}, 1 mM $MgCl_2$ and 0.1% bovine serum albumin (BSA). Cells were incubated with 200 μl of 1 mg ml^{-1} Fluo3-AM (Dojindo, Kumamoto, Japan) for 30 min in the dark. Cells were then rinsed three times in PBS wash solution, as described above, to remove any extra Fluo3-AM. Cells were stimulated with nicotine and levels of calcium influx were measured by FluoroScan (Thermo Fisher Scientific Inc, Waltham, MA, USA). The excitation wavelength was 353 and 373 nm, and the emission wavelength was 510 nm. Non-selective nAChR antagonist, D-tubocurarine, was obtained from Sigma (St. Louis, MO, USA). In some experiments, MPDL22 cells were pretreated with 10^{-4} M D-tubocurarine, which was the most effective concentration for inhibiting nicotine-induced calcium influx in preliminary experiment, for 30 min before calcium measurement.

Mineralization assay
Histochemistry for staining calcified nodules was performed using the alizarin red staining method (Dahl, 1952). Cell layers were washed twice with PBS and then fixed in dehydrated ethanol. After fixation, the cell layers were stained with 1% alizarin red S in 0.1% NH_4OH (pH 6.3–6.5) for 5 min. The dishes were washed with H_2O and then observed microscopically, digitized and analyzed using the WinRoof software program (Mitani Corporation, Fukui, Japan).

Statistical analysis
Results were analyzed for statistical significance using the Student's *t*-test. Differences were considered significant at P values < 0.05.

Results

Expression of nAChRs mRNA and calcium signaling of nAChR in MPDL22 cells
To determine whether nAChRs were expressed in MPDL cells, mRNA was extracted from MPDL22 cells and analyzed by RT-PCR using mouse nAChR-specific primers. As shown in Figure 1a, MPDL22 cells were positive for α3, α4, α7 and β2 nAChR mRNA. To investigate whether the nAChRs expressed were functional, we analyzed cytozolic Ca^{2+} levels using Flou-3AM. When nicotine was used as the agonist for nAChR, it elicited cytozolic Ca^{2+}. Pretreatment with non-selective nAChR antagonist, D-tubocurarine, reduced nicotine-induced calcium mobilization (Figure 1b).

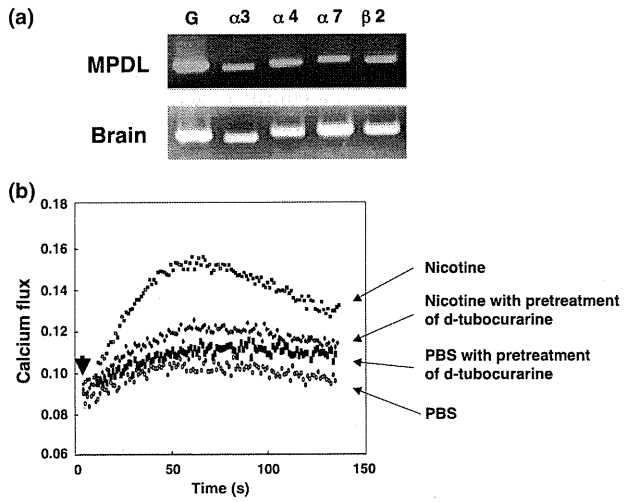

Figure 1 MPDL22 cells express functional nAChRs. **(a)** Expression of nAChR mRNA in MPDL22 cells was examined by RT-PCR. The number of PCR cycles was 33 and 24 for nAChRs and GAPDH, respectively. G: GAPDH. **(b)** Effects of nicotine on calcium mobilization in MPDL22 cells were monitored by measuring the fluorescence ratio (F340/380). Cells were pretreated for 30 min in the presence or absence of non-selective nAChR antagonist, D-tubocurarine (10^{-4} M), before addition of nicotine (10^{-3} M) or PBS. The arrowhead indicates the time of application of the stimulators. The results of one representative experiment from three identical experiments are shown

Effects of nicotine on MPDL22 proliferation

To investigate the effects of nicotine on the proliferation response of MPDL cells, cells were cultured for 48 h in a medium containing 1% FCS with or without nicotine. As previous studies revealed that FGF-2 induced the proliferation of PDL (Takayama *et al*, 1997), FGF-2 concentration of 100 ng ml^{-1}, which was the most optimal concentration for MPDL proliferation in preliminary experiment, was used as a positive control of this assay. The exposure of 10^{-8} M to 10^{-3} M nicotine did not induce significant proliferative responses in MPDL22 cells (Figure 2).

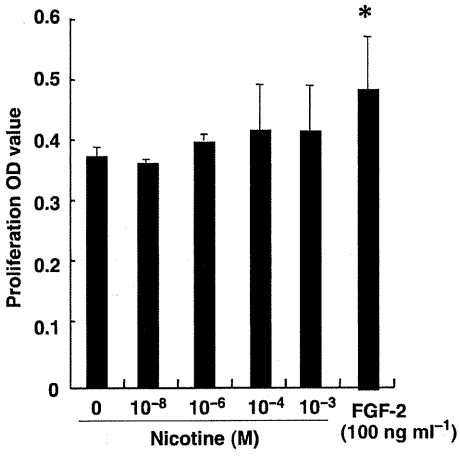

Figure 2 Effects of nicotine on proliferation of MPDL cells. MPDL cells were cultured with various doses of nicotine or FGF-2 (100 ng ml^{-1}) for 2 days. Values are means ± s.d. of four determinations. *$P < 0.05$ compared with medium only

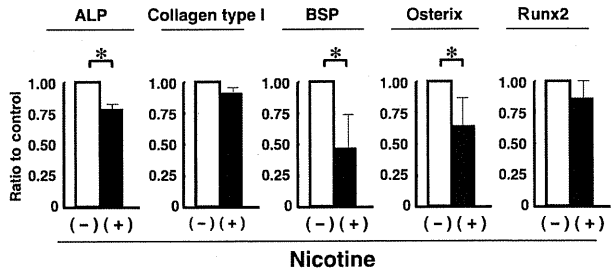

Figure 3 Analysis of mRNA expression of ECM in MPDL cells by RT-PCR. RNA samples were obtained from MPDL cells 2 days after nicotine treatment (10^{-3} M). The relative expression of each gene was standardized against the amount in HPRT as control and the expression of ECM in MPDL cells without nicotine was taken as 1.0. Values are means ± s.d. of three or four determinations. *$P < 0.05$ compared with non-treated

Effects of nicotine on mRNA expression of ALP, BSP and osterix in MPDL22 cells

We then examined the effects of nicotine (10^{-3} M) on gene expression of the extracellular matrix (ECM) and osteoblastic transcription factors (Figure 3). MPDL22 cells, which were treated with nicotine, showed significantly decreased mRNA expression of ALP, BSP and osterix. In addition, the expression of collagen type I and *runx2* were also decreased compared with the control, but not significantly.

Effects of nicotine on mineralized nodule formation in MPDL22 cells

We cultured MPDL22 cells with or without nicotine in mineralization medium and then examined mineralized nodule formation on day 12. As shown in Figure 4a,b, nicotine reduced alizarin red staining intensity. Even a low concentration of nicotine (10^{-8} M) decreased mineralized nodule formation by the MPDL22 cells. Inhibitory effects of nicotine on the mineralization were partly abrogated by pretreatment with D-tubocurarine (Figure 4c). Next, we examined the time dependency of period of nicotine treatment on the inhibition of mineralization of MPDL cells (Figure 5). As shown in Figure 4, treatment with 10^{-3} M nicotine inhibited mineralization of MPDL22 cells. Interestingly, treatment with the same concentration of nicotine only for the first 8 days still considerably inhibited the mineralization. Similarly, nicotine treatment for both first 4 days (sample ID 4: day 0–4) and for the following 4 days (sample ID 5: day 4–8) still inhibited the mineralized nodule formation significantly.

Discussion

Little is known about the expression of nAChR subunits in hard tissue-forming cells. We previously reported that human dental pulp cells express nAChRs (Yanagita *et al*, 2008). In addition, α4 nAChR was expressed in human primary osteoblasts (Walker *et al*, 2001) and a recent study has reported human growth plate chondrocytes express α5, α7, β1 and ε nAChR subunits (Kawakita *et al*, 2008). In this study, we found that

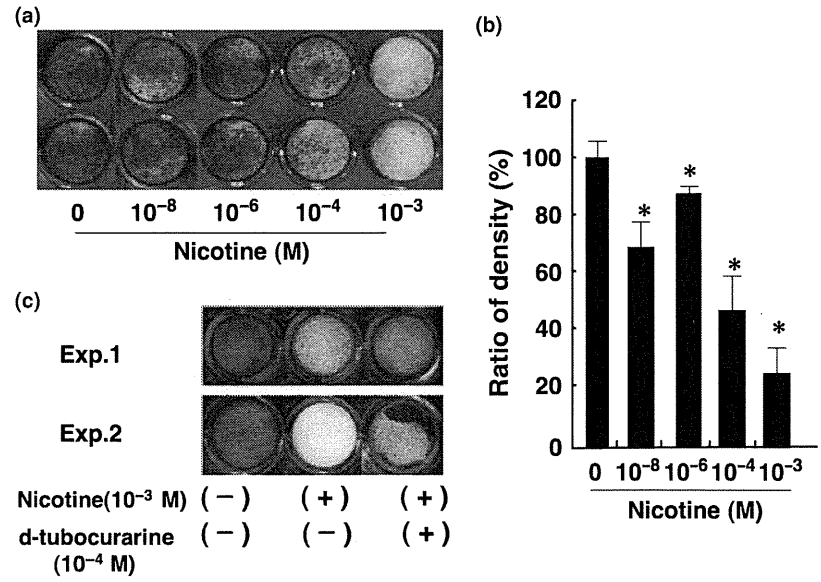

Figure 4 Effects of nicotine on mineralization of MPDL cells. **(a)** Effects of nicotine (10^{-8} M to 10^{-3} M) on mineralization in MPDL cells were examined by alizarin red staining. Alizarin red staining was performed after 12 days of culture in mineralization medium. Results of one representative experiment out of three identical experiments are shown. **(b)** The relative expression value of alizarin staining is shown in **(a)** and was quantitated and normalized to alizarin staining without nicotine. **(c)** Effects of D-tubocurarine on nicotine-dependent inhibition of the mineralization was examined. Alizarin red staining was performed after 12 days of culture in mineralization medium with nicotine (10^{-3} M) in the presence or absence of D-tubocurarine (10^{-4} M). Results of one representative experiment out of three identical experiments are shown. $*P < 0.05$ compared with medium only

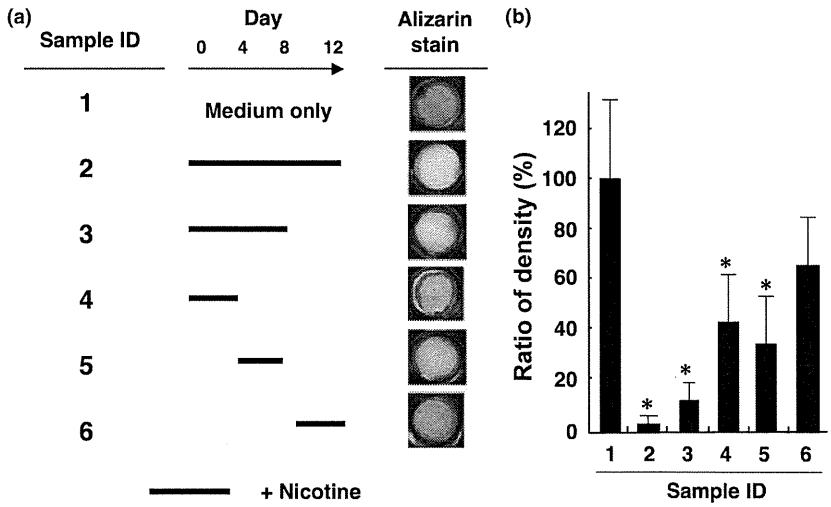

Figure 5 Effect of nicotine at differential stages of mineralization of MPDL cells. **(a)** Nicotine (10^{-3} M) was added to mineralization medium for the indicated periods and alizarin red staining was performed after 12 days of culture. **(b)** The relative expression value of the alizarin staining is shown in **(a)** and was quantitated and normalized to alizarin staining without nicotine. Results of one representative experiment out of two identical experiments are shown. $*P < 0.05$ compared with medium only

expression of α3 α4, α7 and β2 nAChR subunits at mRNA level, which are reportedly the most abundantly expressed subtypes in murine brain and ganglion cells (Gahring and Rogers, 2005; Gotti *et al*, 2006) are detected in MPDL cells by RT-PCR. Unfortunately, we did not reveal the nAChR subunit expression at protein level in this study, and the detection of nAChR subunit proteins by immunoblot or immunohistochemistry remained to be the future work. Furthermore, nicotine elicited a transient calcium influx and D-tubocurarine, a non-selective nAChR antagonist, inhibited the calcium signals. This suggests that the effects of smoking on MPDL cells can be mediated via nAChR.

The results of this study show that nicotine did not change the proliferative responses of MPDL cells. In contrast, it was reported that nicotine has cytotoxicity and inhibits proliferation of human gingival fibroblasts and periodontal ligament cells (Giannopoulou *et al*, 2001; Chang *et al*, 2002). On the contrary, a recent study showed that nicotine increased the proliferation rate of a murine preosteoblastic cell line, MC3T3-E1 (Sato *et al*, 2008). In addition, our previous study revealed that nicotine increased the DNA amounts in human dental pulp cells (Yanagita *et al*, 2008). Thus, the effect of nicotine on cellular proliferation is still controversial and may be cell-type dependent.

We examined the expression of some osteogenic markers, and revealed by RT-PCR that nicotine reduced the mRNA expression of ALP, BSP, and osterix (Figure 3). ALP is an enzyme marker of osteoblasts and participates in bone mineralization (Majeska and Wuthier, 1975). BSP is a small integrin-binding ligand N-linked glycoprotein, involved in the regulation of mineralization (Moses *et al*, 2006). Osterix, the osteoblast-specific transcription factor, has been identified as a modulator of bone formation and osteoblast differentiation (Nakashima and de Crombrugghe, 2003). Thus,

the inhibitory effects of nicotine on the above-mentioned mRNA expression are correlate with that on the mineralization of MPDL22 cells. On the contrary, nicotine-induced BSP and collagen type I mRNA expression but down-regulated osteopontin mRNA in a human osteosarcoma cell line (Tanaka *et al*, 2005). Another study documented that 24-h treatment of nicotine up-regulated collagen type I, ALP and osteocalcin in osteosarcoma cells, but after 48 or 72-h incubation mRNA expression of these three genes was downregulated by nicotine in a dose-dependent manner (Rothem *et al*, 2009). In the case of chondrocytes, nicotine decreased the expression of ALP (Kawakita *et al*, 2008). Thus, the effects of nicotine on the mRNA expression of bone-related ECM also appears to be cell-type dependent.

Alizarin red staining showed that mineralization of MPDL22 cells was inhibited by nicotine (Figure 4a,b), and the inhibition was partly abrogated by D-tubocurarine, a non-selective nAChRs antagonist (Figure 4c). Furthermore, nicotine treatment for the first and second 4 days (sample ID 4, 5: day 0–4, 4–8) inhibited the mineralization. This result suggests that the suppressive effect of nicotine on the cytodifferentiation and mineralization of MPDL22 cells is culture-phase dependent. The fact that nicotine treatment for the last 4 days (sample ID 6: day 8–12) did not reduce the mineralization may suggest that MPDL22 should be committed to terminally differentiate at day 8. As shown in Figure 1b, D-tubocurarine almost completely inhibited nicotine-induced calcium influx, although suppression of mineralization was not completely recovered by the reagent (Figure 4c). In the case of calcium influx experiment, the incubation time was quite short, whereas cells were cultured for 12 days in mineralization assay. It is difficult at this point to establish a correlation between the initial, transient calcium signals and the mineralization results done on day 12. Measurement of calcium levels in the cells at day 12 may need to be done to accurately determine if early, transient calcium signals are linked to mineralization via an unknown signaling cascade.

Recently nicotine has been reported to induce p53 in osteoblasts (Sato *et al*, 2008). p53 is originally identified as a tumor suppressor, and promotes cell cycle arrest (Vogelstein *et al*, 2000). Interestingly it has been demonstrated that p53 regulates osteogenic differentiation (Wang *et al*, 2006). This suggests that p53 may be involved in the nicotine-induced inhibition of the differentiation of MPDL cells. Further studies are required to clarify the nicotine-induced signal cascade through nAChRs that influences the mineralization.

The association between smoking and progression of periodontal diseases, including alveolar bone loss, has been well-investigated (Grossi *et al*, 1994; Grossi *et al*, 1995; Ryder, 2007). Nicotine alters the cellular functions of PDL cells and gingival fibroblasts *in vitro* (Chang *et al*, 2002). Smokers demonstrate impaired periodontal tissue regeneration compared with non-smokers (Stavropoulos *et al*, 2004). The inhibitory effect of nicotine on the mineralization of PDL cells partly accounts for the reason. Furthermore, smokers have been reported to suffer decrease of bone mass, increased risk of fracture and prolonged fracture repair (Krall and Dawson-Hughes, 1991, 1999). The important information is that the nicotine concentration in smokers' sera was 25–444 nM (Russell *et al*, 1980) and that serum nicotine levels of non-smokers exposed to secondhand smoke was around nM (5.9 ng ml^{-1}) (Pacifici *et al*, 1995). Figure 4a showed that a low concentration of nicotine circulating in the blood stream (~10 nM) can negatively influence the mineralization of PDL cells. These results suggest the possibility that secondhand smoke could be detrimental to periodontal health. In addition, inflammatory cytokines are detected in inflamed periodontal lesions, and some of those cytokines such as IL-1β affect ECM expression (Chien *et al*, 1999). Therefore, to investigate the effect of nicotine on cytokine-induce ECM expression should be carried out in the future.

In conclusion, we have shown that nicotine is a potent negative regulator of cytodifferentiation and mineralization in PDL cells. Our studies suggest that nicotine causes progressing periodontal diseases and unfavorable prognoses after periodontal treatments.

Acknowledgements

This work was supported in part by Grants-in-Aid for Scientific Research (No. 2039529, 20390530, 20592427) and the 21st Century COE entitled 'Origination of Frontier BioDentistry' at Osaka University Graduate School of Dentistry supported by the Ministry of Education, Culture, Sports, Science and Technology.

Competing interests

None declared.

Ethical approval

Not required.

References

Chang YC, Huang FM, Tai KW, Yang LC, Chou MY (2002). Mechanisms of cytotoxicity of nicotine in human periodontal ligament fibroblast cultures in vitro. *J Periodontal Res* **37:** 279–285.

Chien HH, Lin WL, Cho MI (1999). Interleukin-1β-induced release of matrix proteins into culture media causes inhibition of mineralization of nodules formed by periodontal ligament cells in vitro. *Calcif Tissue Int* **64:** 402–413.

Dahl LK (1952). A simple and sensitive histochemical method for calcium. *Proc Soc Exp Biol Med* **80:** 474–479.

Feyerabend C, Higenbottam T, Russell MA (1982). Nicotine concentrations in urine and saliva of smokers and non-smokers. *Br Med J (Clin Res Ed)* **284:** 1002–1004.

Gahring LC, Rogers SW (2005). Neuronal nicotinic acetylcholine receptor expression and function on nonneuronal cells. *AAPS J* **7:** E885–E894.

Giannopoulou C, Roehrich N, Mombelli A (2001). Effect of nicotine-treated epithelial cells on the proliferation and

collagen production of gingival fibroblasts. *J Clin Periodontol* **28:** 769–775.

Gotti C, Zoli M, Clementi F (2006). Brain nicotinic acetylcholine receptors: native subtypes and their relevance. *Trends Pharmacol Sci* **27:** 482–491.

Grossi SG, Zambon JJ, Ho AW, Koch G, Dunford RG, Machtei EE, Norderyd OM, Genco RJ (1994). Assessment of risk for periodontal disease. I. Risk indicators for attachment loss. *J Periodontol* **65:** 260–267.

Grossi SG, Genco RJ, Machtei EE, *et al.* (1995). Assessment of risk for periodontal disease. II. Risk indicators for alveolar bone loss. *J Periodontol* **66:** 23–29.

Hoffmann D, Adams JD (1981). Carcinogenic tobacco-specific N-nitrosamines in snuff and in the saliva of snuffdippers. *Cancer Res* **41:** 4305–4308.

Kageyama-Yahara N, Suehiro Y, Yamamoto T, Kadowaki M (2008). IgE-induced degranulation of mucosal mast cells is negatively regulated via nicotinic acetylcholine receptors. *Biochem Biophys Res Commun* **377:** 321–325.

Kawakita A, Sato K, Makino H, *et al.* (2008). Nicotine acts on growth plate chondrocytes to delay skeletal growth through the alpha7 neuronal nicotinic acetylcholine receptor. *PLoS One* **3:** e3945.

Krall EA, Dawson-Hughes B (1991). Smoking and bone loss among postmenopausal women. *J Bone Miner Res* **6:** 331–338.

Krall EA, Dawson-Hughes B (1999). Smoking increases bone loss and decreases intestinal calcium absorption. *J Bone Miner Res* **14:** 215–120.

Lofroth G (1989). Environmental tobacco smoke: overview of chemical composition and genotoxic components. *Mutat Res* **222:** 73–80.

Majeska RJ, Wuthier RE (1975). Studies on matrix vesicles isolated from chick epiphyseal cartilage. Association of pyrophosphatase and ATPase activities with alkaline phosphatase. *Biochim Biophys Acta* **391:** 51–60.

Martinez-Canut P, Guarinos J, Bagan JV (1996). Periodontal disease in HIV seropositive patients and its relation to lymphocyte subsets. *J Periodontol* **67:** 33–36.

Moses KD, Butler WT, Qin C (2006). Immunohistochemical study of small integrin-binding ligand, N-linked glycoproteins in reactionary dentin of rat molars at different ages. *Eur J Oral Sci* **114:** 216–222.

Nakashima K, de Crombrugghe B (2003). Transcriptional mechanisms in osteoblast differentiation and bone formation. *Trends Genet* **19:** 458–466.

Pacifici R, Altieri I, Gandini L, *et al.* (1995). Environmental tobacco smoke: nicotine and cotinine concentration in semen. *Environ Res* **68:** 69–72.

Rothem DE, Rothem L, Soudry M, Dahan A, Eliakim R (2009). Nicotine modulates bone metabolism-associated gene expression in osteoblast cells. *J Bone Miner Metab* **27:** 555–561.

Russell MA, Jarvis M, Iyer R, Feyerabend C (1980). Relation of nicotine yield of cigarettes to blood nicotine concentrations in smokers. *Br Med J* **280:** 972–976.

Ryder MI (2007). The influence of smoking on host responses in periodontal infections. *Periodontol* **43:** 267–277.

Sato T, Abe T, Nakamoto N, *et al.* (2008). Nicotine induces cell proliferation in association with cyclin D1 up-regulation and inhibits cell differentiation in association with p53 regulation in a murine pre-osteoblastic cell line. *Biochem Biophys Res Commun* **377:** 126–130.

Seo BM, Miura M, Gronthos S, *et al.* (2004). Investigation of multipotent postnatal stem cells from human periodontal ligament. *Lancet* **364:** 149–155.

Seow WK, Thong YH, Nelson RD, MacFarlane GD, Herzberg MC (1994). Nicotine-induced release of elastase and eicosanoids by human neutrophils. *Inflammation* **18:** 119–127.

Stavropoulos A, Mardas N, Herrero F, Karring T (2004). Smoking affects the outcome of guided tissue regeneration with bioresorbable membranes: a retrospective analysis of intrabony defects. *J Clin Periodontol* **31:** 945–950.

Takayama S, Murakami S, Miki Y, *et al.* (1997). Effects of basic fibroblast growth factor on human periodontal ligament cells. *J Periodontal Res* **32:** 667–675.

Tanaka H, Tanabe N, Suzuki N, *et al.* (2005). Nicotine affects mineralized nodule formation by the human osteosarcoma cell line Saos-2. *Life Sci* **77:** 2273–2284.

Vogelstein B, Lane D, Levine AJ (2000). Surfing the p53 network. *Nature* **408:** 307–310.

Walker LM, Preston MR, Magnay JL, Thomas PB, El Haj AJ (2001). Nicotinic regulation of c-fos and osteopontin expression in human-derived osteoblast-like cells and human trabecular bone organ culture. *Bone* **28:** 603–608.

Wang X, Kua HY, Hu Y, *et al.* (2006). p53 functions as a negative regulator of osteoblastogenesis, osteoblast-dependent osteoclastogenesis, and bone remodeling. *J Cell Biol* **172:** 115–125.

Yamada S, Tomoeda M, Ozawa Y, *et al.* (2007). PLAP-1/asporin: a novel negative regulator of periodontal ligament mineralization. *J Biol Chem* **282:** 23070–23080.

Yanagita M, Kashiwagi Y, Kobayashi R, Tomoeda M, Shimabukuro Y, Murakami S (2008). Nicotine inhibits mineralization of human dental pulp cells. *J Endod* **34:** 1061–1065.

Supplemental Material can be found at:
http://www.jbc.org/content/suppl/2010/07/15/M109.097303.DC1.html

THE JOURNAL OF BIOLOGICAL CHEMISTRY VOL. 285, NO. 36, pp. 28286–28297, September 3, 2010
© 2010 by The American Society for Biochemistry and Molecular Biology, Inc. Printed in the U.S.A.

Role of Mechanical Stress-induced Glutamate Signaling-associated Molecules in Cytodifferentiation of Periodontal Ligament Cells*[S]

Received for publication, December 20, 2009, and in revised form, June 23, 2010 Published, JBC Papers in Press, June 24, 2010, DOI 10.1074/jbc.M109.097303

Chiharu Fujihara[‡1], Satoru Yamada[‡1], Nobuhiro Ozaki[‡], Nobuo Takeshita[§], Harumi Kawaki[§], Teruko Takano-Yamamoto[§], and Shinya Murakami[‡2]

From the [‡]Department of Periodontology, Division of Oral Biology and Disease Control, Osaka University Graduate School of Dentistry, 1-8 Yamadaoka, Suita, Osaka 565-0871, Japan and the [§]Division of Orthodontics and Dentofacial Orthopedics, Department of Oral Health and Development Sciences, Tohoku University Graduate School of Dentistry, 4-1 Seiryo-machi, Aoba-ku, Sendai 980-8578, Japan

In this study, we analyzed the effects of tensile mechanical stress on the gene expression profile of *in vitro*-maintained human periodontal ligament (PDL) cells. A DNA chip analysis identified 17 up-regulated genes in human PDL cells under the mechanical stress, including *HOMER1* (homer homolog 1) and *GRIN3A* (glutamate receptor ionotropic *N*-methyl-D-aspartate 3A), which are related to glutamate signaling. RT-PCR and real-time PCR analyses revealed that human PDL cells constitutively expressed glutamate signaling-associated genes and that mechanical stress increased the expression of these mRNAs, leading to release of glutamate from human PDL cells and intracellular glutamate signal transduction. Interestingly, exogenous glutamate increased the mRNAs of cytodifferentiation and mineralization-related genes as well as the ALP (alkaline phosphatase) activities during the cytodifferentiation of the PDL cells. On the other hand, the glutamate signaling inhibitors riluzole and (+)-MK801 maleate suppressed the alkaline phosphatase activities and mineralized nodule formation during the cytodifferentiation and mineralization. Riluzole inhibited the mechanical stress-induced glutamate signaling-associated gene expressions in human PDL cells. Moreover, *in situ* hybridization analyses showed up-regulation of glutamate signaling-associated gene expressions at tension sites in the PDL under orthodontic tooth movement in a mouse model. The present data demonstrate that the glutamate signaling induced by mechanical stress positively regulates the cytodifferentiation and mineralization of PDL cells.

The ability of cells to sense and respond to physical stress is required for tissue homeostasis and normal development. In muscle, bone, tendon, periodontium, and the cardiovascular system, applied forces of physiological magnitude regulate cellular processes that are critical for normal tissue and organ functions, such as differentiation, proliferation, and migration (1). The periodontal ligament (PDL)[3] is a connective tissue interposed between the roots of teeth and the inner wall of the tooth-supporting bone (alveolar bone) socket. The PDL constitutively and iatrogenically receives mechanical stress, such as occlusal pressure and orthodontic forces, which have effects on the homeostasis of the PDL (2). Proper mechanical stress on teeth induces not only the proliferation and differentiation of PDL cells into osteoblasts and cementoblasts but also the synthesis and degradation of extracellular matrix (ECM) molecules (3). For example, during orthodontic tooth movement, two types of sites (tension sites and pressure sites) arise around the tooth through the orthodontic force. At the tension sites, the PDL is stretched, and the expressions of bone-related genes, such as osteocalcin (4) and bone sialoprotein (5), are up-regulated, such that bone formation is finally induced on the alveolar bone facing the tooth root (6). On the other hand, at the pressure sites, the PDL is compressed, and osteoclasts are activated. Consequently, resorption of the alveolar bone is induced. An orchestrated balance between bone formation and resorption controls tooth movement (7). In contrast, elimination of mechanical stress on teeth is known to cause atrophy of the PDL *in vivo* (8). Kaneko *et al.* (9) reported that loss of occlusal function by extraction of the antagonistic upper molars of rats caused atrophic changes in the PDL of the lower molars, such as narrowing of the space, disorientation of collagen fibers, and decreases in proteoglycans. These findings indicate that mechanical stress on teeth affects the remodeling of the PDL, cementum, and alveolar bone. Thus, it is important to clarify the physiological functions of mechanical stress on the PDL.

To clarify the molecular basis of the mechanical stress-regulated PDL functions, we analyzed the gene expression profile of human PDL cells receiving tensile mechanical stress *in vitro*. Interestingly, an oligo-DNA chip analysis identified two glutamate signaling-associated genes, *HOMER1* (homer homolog 1) and *GRIN3A* (glutamate receptor ionotropic *N*-methyl-D-aspartate 3A), among the up-regulated genes. L-Glutamate is the most abundant amino acid in the central nervous system and plays important roles in neurotransmission (10). Stimulation of

* This work was supported by Grants-in-aid 20390529 and 20390530 from the Japan Society for the Promotion of Science and Research Grant H21-001 from the Ministry of Health, Labor, and Welfare.

[S] The on-line version of this article (available at http://www.jbc.org) contains supplemental Tables 1 and 2.

[1] These authors contributed equally to this work.

[2] To whom correspondence should be addressed. Tel.: 81-6-6879-2930; Fax: 81-6-6879-2934; E-mail: ipshinya@dent.osaka-u.ac.jp.

[3] The abbreviations used are: PDL, periodontal ligament; MK801, (+)-MK801 maleate; CREB, cAMP-response element-binding protein; ECM, extracellular matrix; Ca^{2+}, calcium ion; NMDAR, *N*-methyl-D-aspartate receptor; IP_3, inositol 1,4,5-trisphosphate; aRNA, amino allyl RNA; DIG, digoxigenin.

Downloaded from www.jbc.org at OSAKA UNIVERSITY, on May 10, 2011

presynaptic cells promotes the release of glutamate, and the released glutamate induces glutamate signaling by binding to glutamate receptors on the postsynaptic cells. In addition to the central nervous system, glutamate signaling has been observed in non-neural tissues, such as the taste buds (11), spleen (12), and bone (13), and modulates various functions of each tissue (14). However, involvement of glutamate signaling in the PDL has not been reported. In the present study, we further analyzed the gene expression and functions of glutamate signaling-associated molecules in PDL cells to elucidate the roles of glutamate signaling in the PDL.

EXPERIMENTAL PROCEDURES

Reagents—α-Modified Eagle's medium was obtained from Nikken Biomedical Laboratory (Kyoto, Japan). Fetal calf serum (FCS) was purchased from JRH Biosciences (Lenexa, KS). Riluzole, bisbenzimidazole (Hoechst 33258), and DNA sodium salt (from calf thymus) were products from Sigma. Kanamycin, L-glutamate, β-glycerophosphate, ascorbic acid, and *p*-nitrophenyl phosphate were obtained from Wako Pure Chemical Industries (Osaka, Japan). (+)-MK801 maleate (MK801) was purchased from Tocris Cookson (Bristol, UK).

Cell Culture—Human PDL cells were isolated as described previously (15). The cells were cultured in α-modified Eagle's medium supplemented with 10% FCS, 50 units/ml penicillin G, and 50 μg/ml streptomycin at 37 °C under 5% CO_2. For the induction of cytodifferentiation, human PDL cells were cultured in α-modified Eagle's medium with 10% FCS in the presence of 10 mM β-glycerophosphate and 50 μg/ml ascorbic acid (mineralization-inducing medium). The mineralization-inducing medium was replaced every 3 days.

Application of Mechanical Stress—To allow cell attachment, 10-cm^2 silicon membrane chambers (Scholertec, Osaka, Japan) were coated with 0.3 mg/ml pepsin-digested collagen type I derived from swine (Nitta Gelatin, Osaka, Japan) according to the Scholertec manufacturer's instructions. Human PDL cells were transferred to the chambers at a density of 1.5×10^4 cell/cm^2 and cultured in α-modified Eagle's medium with 10% FCS for 3 days. The chambers were applied to a stretch apparatus, Scholertec NS-350 (Scholertec), and the cells were repeatedly stretched and relaxed at 37 °C under 5% CO_2 *in vitro*. The force conditions were 0.5 Hz (30 cycles/min) with 110% elongation for 0, 24, and 48 h. This force represented the physiological conditions of occlusal force (16). Cells seeded on the chambers without stretching served as controls.

Oligo-DNA Chip Analysis—Total RNA (1 μg) extracted from the stretched human PDL cells using RNA Bee (Tel-Test Inc., Friendswood, TX) was targeted to synthesize experimental amino allyl RNA (aRNA) using an Amino Allyl MessageAmp aRNA kit (Ambion Inc., Austin, TX) according to the manufacturer's protocol. Cy3 or Cy5 fluorescent dyes (Amersham Biosciences) were incorporated into the aRNAs by an indirect labeling method. The labeled aRNAs were fragmented and hybridized to an AceGene Human Oligo Chip 30K (Hitachi Software Engineering Co., Ibaraki, Japan) consisting of 30,000 human oligonucleotide features. After a 12-h hybridization, the DNA chip was washed according to the manufacturer's instructions, and the fluorescence intensities were scanned with a ScanArray Lite (PerkinElmer Life Sciences). The resulting image was analyzed using Scan Array Express version 2.0. Normalization using LOWELL was performed for data obtained from the raw data.

Real-time RT-PCR Analysis—cDNA was synthesized from the purified total RNA using a high capacity cDNA reverse transcription kit (Applied Biosystems, Carlsbad, CA) according to the manufacturer's instructions. The obtained cDNA was mixed with Power PCR SYBR Master Mix (Applied Biosystems) and gene-specific primers (Takara Bio, Shiga, Japan). The sequences of the primers are shown in supplemental Table 1. Real-time PCR was performed using a 7300 fast real-time RT-PCR system (Applied Biosystems) according to the manufacturer's instructions. The amplification conditions consisted of an initial 15-min denaturation step at 95 °C, followed by 40 cycles of denaturation at 94 °C for 15 s, annealing at 60 °C for 30 s, and elongation at 72 °C for 30 s. The dissociation curves were analyzed to ensure the amplification of a single PCR product. Three independent assays were performed for each primer. The amount of cDNA was calculated for each sample from the standard curve. The relative expression is shown after normalization by the gene expression of *HPRT* (hypoxanthine phosphoribosyltransferase).

Conventional RT-PCR Analysis—The purified total RNA was reverse-transcribed with SuperScript II reverse transcriptase (Invitrogen) and an oligo(dT) primer (Invitrogen). The synthesized cDNA was mixed with AmpliTaq Gold DNA polymerase (Applied Biosystems) and gene-specific primers synthesized by GeneDesign Inc. (Osaka, Japan). The sequences of the primers are shown in supplemental Table 2. PCR was performed using a PTC-200 Peltier thermal cycler (Bio-Rad). The amplification conditions consisted of an initial incubation at 94 °C for 9 min, followed by cycles of denaturation at 94 °C for 60 s, annealing at the temperatures indicated in supplemental Table 2, and elongation at 72 °C for 60 s. The PCR products were evaluated by agarose gel electrophoresis.

Determination of Released Glutamate—The levels of glutamate were determined by a modification of an enzyme-linked fluorimetric assay according to a previously published protocol (17). In the presence of glutamate dehydrogenase (Oriental Yeast Co., Osaka, Japan) and β-nicotinamide adenine dinucleotide phosphate (β-$NADP^+$) (Oriental Yeast Co.), released glutamate is oxidized to α-ketoglutarate with the production of NADPH, which can be determined fluorometrically to quantify the glutamate concentration. Briefly, human PDL cells were grown in 6-well plates or stretched on chambers. The supernatants were collected from each well, filtered with a Minisart 0.2-μm filter (Sartorius Stedim Biotech, Goettingen, Germany), and prewarmed to 25 °C with 7 mM β-$NADP^+$ (pH 7.4). The reaction was initiated by the addition of glutamate dehydrogenase (9 IU/ml). After incubation for 15 min, the absorbance was measured at 320 nm using a GeneQuant pro"S" spectrophotometer (Amersham Biosciences) and compared with standard curves constructed using known concentrations of L-glutamate. The DNA concentrations in the cell layers were determined by subtracting the amount of glutamate in the medium as the absorbance of the background in advance.

Downloaded from www.jbc.org at OSAKA UNIVERSITY, on May 10, 2011

A.

Description	Symbol	Ratio
homer homolog 1	*HOMER1*	8.12
ciliary neurotrophic factor receptor	*CNTFR*	6.32
matrix metallopeptidase 15	*MMP15*	5.24
unknown		3.76
unknown		3.46
down syndrome critical region gene 1	*DSCR1*	2.81
leucin rich repeat interacting protein 1	*LRRFIP1*	2.85
KIAA1409	*KIAA1409*	2.68
glutamate receptor ionotropic N-methyl-D-aspartate 3A	*GRIN3A*	2.50
KIAA1799	*KIAA1799*	2.50
mucin 4	*MUC4*	2.29
unknown		2.29
mannosyl-glycoprotein beta-1,6-N-acetyl-glucosaminyltransferase	*MGAT5*	2.29
plexin D1	*PLXND1*	2.24
unknown		2.18
angiopoietin-like 1	*ANGPTL1*	2.11
TP53TG3 protein		2.10

B.

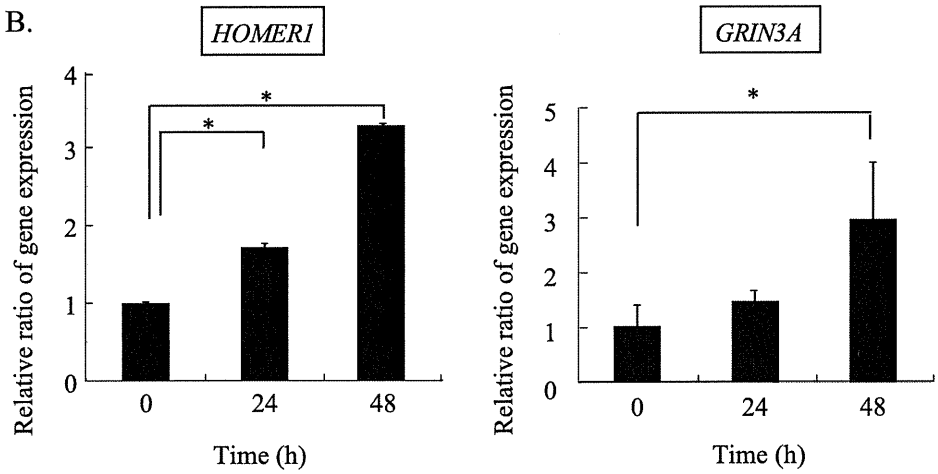

FIGURE 1. **Gene expression profile of human PDL cells under mechanical stress.** *A*, the oligo-DNA chip analysis revealed the gene expression profile of human PDL cells after the application of mechanical stress for 48 h. The ratios are the relative ratio of each gene expression in the 48-h stretched cells to that in the non-stretched cells. *B*, real-time RT-PCR was performed for the gene expressions of *HOMER1* and *GRIN3A* in human PDL cells after the application of mechanical stress for 0, 24, and 48 h. The expressions of *HOMER1* and *GRIN3A* were normalized by the expression of *HPRT*. The values are shown as the relative ratios to 0 h. Values represent the means ± S.D. (*error bars*) of triplicate assays. Similar results were obtained in three separate experiments, and representative data are shown. *, $p < 0.05$, compared with 0 h.

Western Blotting Analysis of Phosphorylation of cAMP-response Element-binding Protein (CREB) in Human PDL Cells—Human PDL cells stimulated by glutamate or mechanical stress were lysed with cell lysis buffer (50 mM Tris-HCl, pH 7.4; 1% Nonidet P-40; 0.25% sodium deoxycholate; 150 mM NaCl; 1 mM EDTA; 1 mM PMSF; 1 mg/ml aprotinin, leupeptin, and pepstatin; 1 mM Na_3VO_4; 1 mM NaF; 1 μM microcystin). The protein concentrations of the cell lysates were measured using a BCA protein assay kit (Pierce) according to the manufacturer's instructions. The cell lysates were subjected to 7.5% SDS-PAGE and then electroblotted onto polyvinylidene difluoride membranes. A rabbit anti-phospho-CREB antibody (1:1000; Millipore, Temecula, CA) and a rabbit anti-CREB antibody (1:1000, Millipore) were used as the primary antibodies. A horseradish peroxidase-linked goat anti-rabbit IgG antibody (Cappel, Aurora, OH) was used as the secondary antibody. Immunoreactive proteins were detected using an ECL Plus kit (GE Healthcare).

Measurement of Intracellular Ca^{2+} Content—Fluorescence measurements of the intracellular Ca^{2+} contents were performed using a Fluoskan Ascent FC spectrophotometer (Thermo Fisher Scientific Inc., Waltham, MA) and a Calcium Kit-Fluo 3 (Dojindo Laboratories, Kumamoto, Japan) according to the manufacturers' protocols. Briefly, human PDL cells were seeded at a density of 1.5×10^4 cells/well on a black 96-well plate. After incubation for 24 h, the cells were washed with PBS and incubated in loading buffer containing Fluo 3-AM for 1 h. The cells were washed with PBS, and then 100 μl of recording medium containing 0.04% Pluronic F-127 and 1.25 mM probenecid was added to each well. The PDL cells were then stimulated with 20 μl of L-glutamate (600 μM). The fluorescence intensities were immediately measured at 1-s intervals using wavelengths of 485 nm for excitation and 538 nm for emission.

Cell Survival Analysis—Human PDL cells were seeded on 12-well dishes at a density of 1.0×10^5 cells/well. After 24 h of serum starvation, the cells were cultured in the presence or absence of inhibitors at specified concentrations for 0, 24, and 48 h. The cells were then treated with trypsin for 5 min at 37 °C and centrifuged at 1,200 × *g* for 5 min. The cell pellets were resuspended with PBS. The live and dead cells were manually counted with a hemocytometer after 0.5% trypan blue staining.

Determination of ALP (Alkaline Phosphatase) Activity—ALP activities were measured according to the procedure described by Bessey *et al.* (18). Briefly, human PDL cells were placed in 12-well plates at a density of 1.0×10^5 cells/well. After two washes with PBS, the cells were sonicated in 2 ml of distilled water at 4 °C. Next, 500 μl of Tris-HCl (1.0 M, pH 9.0), 100 μl of $MgCl_2$ (5 mM), and 150 μl of Triton X-100 (0.04%) were mixed with 150 μl of the supernatants. The addition of 100 μl of *p*-nitrophenyl phosphate (5 mM) as a substrate was used to deter-

Downloaded from www.jbc.org at OSAKA UNIVERSITY, on May 10, 2011

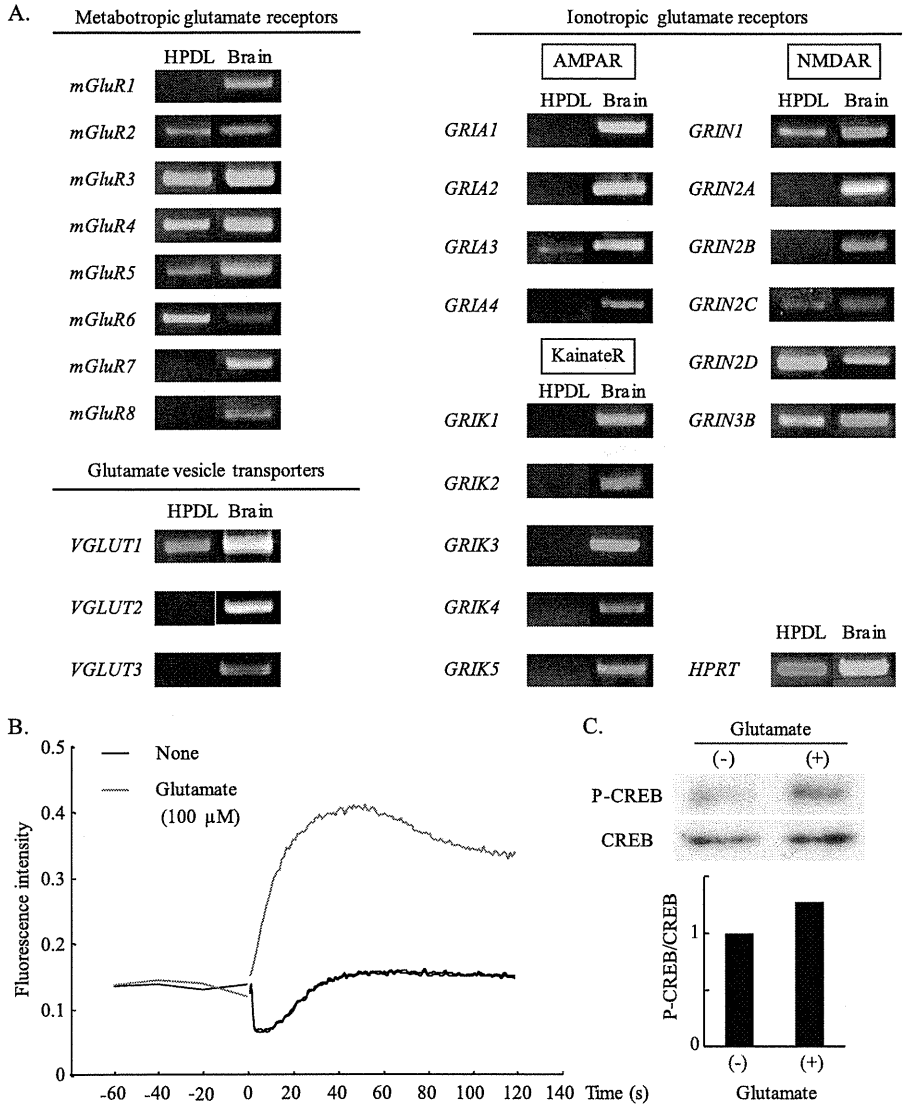

FIGURE 2. **Gene expressions and functions of glutamate signaling-associated molecules in human PDL cells.** *A*, human PDL cells were harvested for RNA isolation, followed by RT-PCR for the gene expressions of glutamate signaling-associated molecules. RNA derived from the human brain was used as a positive control. The numbers of PCR cycles were 40 for metabotropic glutamate receptors and 35 for ionotropic glutamate receptors and glutamate vesicle transporters. The number of PCR cycles was 30 for *HPRT*. Representative results of three independent experiments are shown. *B*, human PDL cells were labeled with the Ca^{2+} fluorescent agent Fluo 3-AM and stimulated with 100 μM exogenous glutamate. The fluorescence intensity was measured to assess the intracellular Ca^{2+} influx. *Black line* (*None*), distilled water alone; *red* (*Glutamate*), glutamate (100 μM). Representative results of four independent experiments are shown. *C*, human PDL cells were stimulated with glutamate (500 μM) for 40 min and then lysed. The cell lysates were subjected to SDS-PAGE and transferred to a membrane that was simultaneously probed with antibodies against phospho-CREB (*P-CREB*) and CREB protein. A quantitative Western blotting analysis is shown as the ratios of the intensities of phospho-CREB and CREB. Representative results of three independent experiments are shown.

mine the ALP activities. The samples were incubated at 37 °C for 30 min, and 0.25 ml of 1 N NaOH was added to stop the reaction. The absorbance of each sample was measured at 405 nm using a microplate reader (model 680; Bio-Rad). One unit of activity was defined as the enzyme activity hydrolyzing 1 nmol of *p*-nitrophenyl phosphate in 30 min.

Determination of Cellular DNA Contents—The DNA content was measured by a modification of the method of Labarca and Paigen (19). Briefly, human PDL cells were washed twice with PBS and sonicated on ice in 2 ml of distilled water. Hoechst 33258 was prepared by dissolution in NaCl (2 M) plus Tris-HCl (25 mM, pH 7.5), and 25 μl of the resulting Hoechst 33258 solution (5 μg/ml) was added to 100 μl of the supernatants. The fluorescence was monitored at an emission wavelength of 450 nm after excitation at 356 nm using a spectrophotometer (Fluoskan Ascent FC, Thermo Fisher Scientific Inc.). The concentration of DNA in the samples was determined by a standard curve based on various concentrations of calf thymus DNA.

Alizarin Red Staining—Histochemical staining of Ca^{2+} was performed by a modification of the method described by Dahl (20). Briefly, human PDL cell layers were washed twice with PBS and then fixed with dehydrated ethanol for 10 min. After fixation, the cell layers were stained with 1% alizarin red S (Wako Pure Chemical Industries) in 0.1% NH_4OH (pH 6.5) for 5 min. The wells were washed with distilled water and scanned with a GT-9700F system (Epson, Nagano, Japan). The density of calcified nodules in each well was calculated using the software Win ROOF version 5.6 (Mitani, Fukui, Japan).

Preparation of a Mouse Mechanical Stimulation Model by Experimental Tooth Movement and Tissue Preparation—The first molars of 6-week-old male ICR mice were moved according to the method described Sakai *et al.* (21). Briefly, a nickel-titanium wire, 0.012 inches in diameter, was fixed to the maxillary incisor with resin, and the right maxillary first molar was moved toward the palatal side for 3 days. The force loaded was directly measured on a plaster model before and after the placement of the wire in each mouse using a dial tension gauge (DTG-10NP, Mitutoyo (Kawasaki, Japan)). A 10-g force was applied to the tooth at 0 h, and no further adjustment was necessary during the 3 days. The animals were anesthetized and perfused with 4% paraformaldehyde (pH 7.4). Samples of the alveolar bone region were prepared at 12 and 24 h after the initiation of experimental tooth movement and fixed in the above solution for ~24 h at 4 °C. The specimens were decalcified in 20% EDTA for 14 days at 4 °C, dehydrated, and embedded in paraffin. The resulting tissue blocks were cut into 7-μm-thick cross-sections and mounted on triethoxyaminopropylsilane-coated slides. The experimental protocol was approved by the Animal Committee of Tohoku University.

Downloaded from www.jbc.org at OSAKA UNIVERSITY, on May 10, 2011

355
70

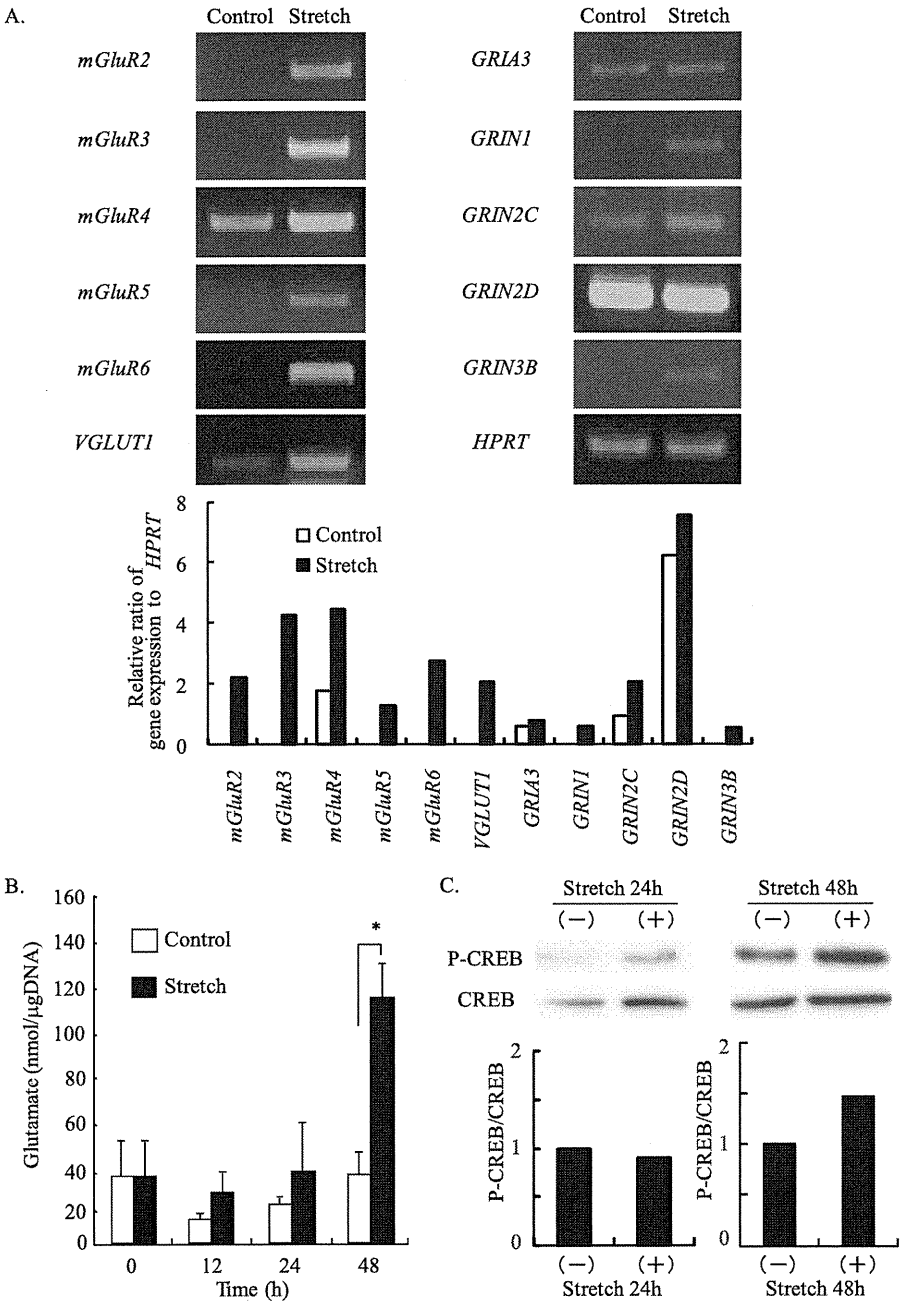

FIGURE 3. **Effects of human PDL cells under mechanical stress on glutamate signaling.** *A*, RT-PCR analyses were performed for the expressions of glutamate signaling-associated genes in human PDL cells after the application of mechanical stress for 24 h. The numbers of PCR cycles were 35 for *mGluR2-R6* and *VGLUT1*, 30 for *GRIA3* and *HPRT*, 40 for *GRIN1* and *GRIN3B*, and 38 for *GRIN2C* and *GRIN2D*. A quantitative analysis of the PCR products using the software Win ROOF is shown as the ratio of the intensities of each gene expression and *HPRT*. *Control*, non-stretched human PDL cells; *Stretch*, stretched cells. Representative results of three independent experiments are shown. *B*, the release of glutamate was determined in supernatants from human PDL cells after the application of mechanical stress for the indicated times. Values are shown as the relative ratios to 0 h. Values represent the means ± S.D. (*error bars*) of triplicate assays. Similar results were obtained in three separate experiments, and representative data are shown. *, $p < 0.05$, compared with non-stretched cells. *C*, Western blotting analysis was carried out for phospho-CREB (*P-CREB*) and CREB proteins in human PDL cells after the application of mechanical stress for the indicated times. A quantitative analysis is shown as the ratios of the intensities of phospho-CREB and CREB. Similar results were obtained in three separate experiments, and representative data are shown.

Probe Preparation—Commercial mouse *Homer1*, *Vlgut1*, *Grin1* (glutamate receptor ionotropic *N*-methyl-D-aspartate 1), *mGluR3* (metabotropic G-protein-coupled receptor 3), *mGluR5*, and *mGluR6* full-length cDNA clones were purchased from Source BioScience Plc Geneservice (Cambridge, England). By using these clones as templates for RT-PCR, we obtained the corresponding cDNA fragments. The DNA fragment for *Homer1* was 501 bp (site location from 388 to 888 bp of accession number NM_147176), that for *Vglut1* (vesicular glutamate transporter 1) was 364 bp (site location from 515 to 878 bp of accession number NM_182993), that for *Grin1* was 478 bp (site location from 1 to 477 bp of accession number NM_008169), that for *mGluR3* was 509 bp (site location from 202 to 710 bp of accession number NM_181850), that for *mGluR5* was 505 bp (site location from 98 to 602 bp of accession number NM_001081414), and that for *mGluR6* was 485 bp (site location from 58 to 542 bp of accession number NM_173372). The DNA fragment for mouse *Runx2* was 701 bp (site location from 3324 to 4024 bp of accession number NM_001146038), that for mouse osteocalcin was 403 bp (site location from 39 to 441 bp of accession number NM_007541), and that for mouse type I collagen was 241 bp (site location from 119 to 359 bp of accession number NM_007742). The fragments were subcloned into pGEM-T Easy vectors (Promega, Madison, WI) and used to generate sense and antisense probes. Digoxigenin (DIG)-11-UTP-labeled single-stranded RNA probes were prepared using a DIG RNA labeling kit (Roche Applied Science) according to the manufacturer's instructions.

In Situ Hybridization—*In situ* hybridization was performed as described previously (4), with minor modifications. Briefly, sections were deparaffinized and fixed with 4% paraformaldehyde for 20 min at room temperature. The sections were then washed and incubated with 5 μg/ml proteinase K (Roche Applied Science) in 10 mM Tris-HCl (pH 8) and 1 mM EDTA for 15 min at room temperature. The sections were refixed, treated with 0.2 N HCl for 10 min at room temperature, washed again, and equilibrated with 0.1 M triethanolamine-HCl buffer (pH 8) for 2 min. Acetylation of the sections was performed by incubation with freshly prepared 0.25% acetic anhydride for 10 min at room temperature. The sections were dehydrated and used

Downloaded from www.jbc.org at OSAKA UNIVERSITY, on May 10, 2011

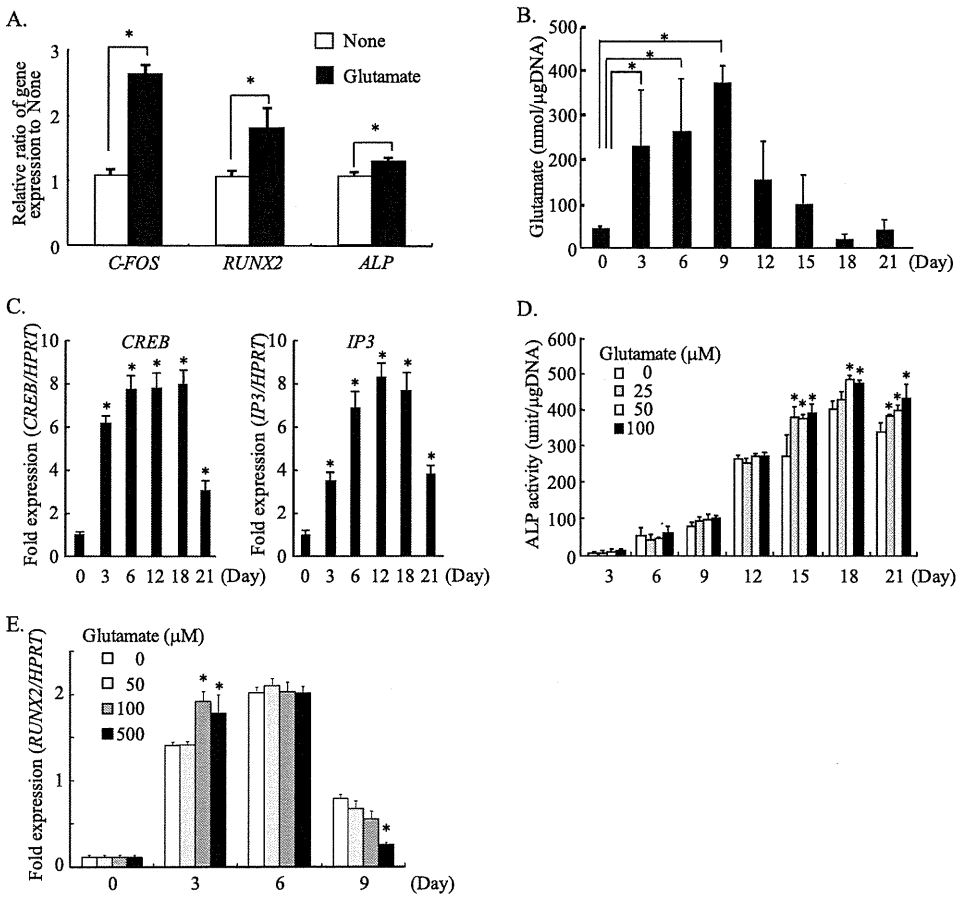

FIGURE 4. **Functional analysis of glutamate signaling in human PDL cells.** *A*, real-time RT-PCR was performed for the expressions of cytodifferentiation- and mineralization-related genes, such as *C-FOS*, *RUNX2*, and *ALP*, after a 12-h stimulation with exogenous glutamate (100 μM). The expressions of *C-FOS*, *RUNX2*, and *ALP* were normalized by the *HPRT* expression. Values are shown as the relative ratios to the non-stimulated controls. Values represent the means ± S.D. (*error bars*) of triplicate assays. Similar results were obtained in three separate experiments, and representative data are shown. *, $p < 0.05$, compared with PBS alone. *B*, human PDL cells were cultured in the mineralization-inducing medium. Every 3 days, the supernatants of the cultured cells were harvested, and the released glutamate was determined. Values represent the means ± S.D. of triplicate assays. Similar results were obtained in three separate experiments, and representative data are shown. *, $p < 0.05$, compared with day 0. *C*, real-time RT-PCR was performed for the expressions of CREB and IP_3 transcripts during the cytodifferentiation and mineralization of human PDL cells. The expressions of CREB and IP_3 were normalized by the *HPRT* expression. Values are shown as the relative ratios to day 0. Values represent the means ± S.D. of triplicate assays. Similar results were obtained in three separate experiments, and representative data are shown. *, $p < 0.01$, compared with day 0. *D*, human PDL cells were cultured in the mineralization-inducing medium in the presence of exogenous glutamate, followed by measurement of the ALP activities during the cytodifferentiation of human PDL cells. Values represent the means ± S.D. of triplicate assays. Similar results were obtained in three separate experiments, and representative data are shown. *, $p < 0.05$, compared with 0 μM glutamate. *E*, real-time RT-PCR was performed for the expression of *RUNX2* during the cytodifferentiation of human PDL cells. Values represent the means ± S.D. of triplicate assays. Similar results were obtained in three separate experiments, and representative data are shown. *, $p < 0.05$, compared with 0 μM glutamate.

for hybridization. Briefly, 0.5 μg/ml of a DIG-UTP-labeled RNA probe was incubated at 85 °C for 3 min after dilution with hybridization solution, and the hybridization solution was then placed on the sections. The sections were covered with Parafilm and incubated at 52 °C for 16 h in a moist chamber saturated with 50% formamide. Next, the Parafilm was dislodged with 5× SSC at 50 °C, and the sections were sequentially incubated with 50% formamide in 2× SSC for 30 min at 52 °C and TNE buffer for 10 min. RNase A treatment (10 μg/ml) was carried out at 37 °C in TNE buffer for 30 min. After washing with 2× SSC and 0.2× SSC twice for 15 min at 52 °C, the sections were incubated with DIG Buffer 1 for 2 min and then with 1.5% blocking reagent in DIG Buffer 1 for 60 min at room temperature. A 100 μl/cm^2 specimen of diluted polyclonal sheep ALP-coupled anti-DIG Fab fragment (1:100–1:150) in DIG Buffer 1 was mounted on the sections and incubated for 30 min at room temperature. After the immunoreaction, the sections were washed twice with DIG Buffer 1 for 15 min and equilibrated with DIG Buffer 3 for 3 min. A coloring solution containing 337.5 μg/ml nitro blue tetrazolium salt and 165 μg/ml 5-bromo-4-chloro-3-indolyl-phosphate in DIG Buffer 3 was mounted on the sections and incubated at 4 °C for 12 h.

Statistical Analysis—Data were expressed as the mean ± S.D. The statistical significance of differences between two means was examined by one-way analysis using Student's *t* test with the Bonferroni correction for multiple comparisons. *p* values of less than 0.05 were considered to indicate a significant difference.

RESULTS

Gene Expression Profile of Human PDL Cells under Mechanical Stress—First, we confirmed the application system of tensile mechanical stress to human PDL cells. After the application of tensile mechanical stress for 48 h, the axes of human PDL cells were aligned perpendicularly to the direction of the stretch force, whereas the control cells were aligned randomly (data not shown). To biologically evaluate whether the mechanical stress worked on human PDL cells in this system, we examined the gene expression of *C-FOS* (FBJ murine osteosarcoma viral oncogene homolog), which is known to be a mechanical stress-responsive gene (22). Real-time PCR analysis showed that the application of mechanical stress to human PDL cells for 48 h significantly up-regulated the gene expression of *C-FOS* (data not shown). Next, utilizing oligo-DNA chips, we analyzed the gene expression profile of human PDL cells after the application of mechanical stress for 48 h. The DNA chip analysis identified 17 up-regulated genes showing at least 2-fold differences in their relative intensities between the stretched cells and the non-stretched control cells (Fig. 1*A*). The full data are also accessible through the NCBI Gene Expression Omnibus (GEO) GSE19118. These results included the following genes with specific functions: for signal

Downloaded from www.jbc.org at OSAKA UNIVERSITY, on May 10, 2011